Coming of Age in the Dark Sector: How Dark Matter Haloes grow their Gravitational Potential Wells

Frank C. van den Bosch[1][*], Fangzhou Jiang[1], Andrew Hearin[2], Duncan Campbell[1], Douglas Watson[3][†], Nikhil Padmanabhan[2]

[1] *Department of Astronomy, Yale University, PO. Box 208101, New Haven, CT 06520-8101*
[2] *Department of Physics, Yale University, 260 Whitney Avenue, New Haven, CT 06520*
[3] *Kavli Institute for Cosmological Physics, University of Chicago, 933 East 56th Street, Chicago, IL 60637*

ABSTRACT
We present a detailed study of how dark matter haloes assemble their mass and grow their (central) potential well. We characterize these via their mass accretion histories (MAHs) and potential well growth histories (PWGHs), which we extract from the Bolshoi simulation and from semi-analytical merger trees supplemented with a method to compute the maximum circular velocity, $V_{\max}$, of progenitor haloes. The results of both methods are in excellent agreement, both in terms of the average and the scatter. We show that the MAH and PWGH are tightly correlated, and that growth of the central potential precedes the assembly of mass; the maximum circular velocity is already half the present day value by the time the halo has accreted only 2 percent of its final mass. Finally, we demonstrate that MAHs have a universal form, which we use to develop a new and improved universal model that can be used to compute the average or median MAH and PWGH for a halo of any mass in any ΛCDM cosmology, without having to run a numerical simulation or a set of halo merger trees.

Key words: methods: analytical — methods: statistical — galaxies: formation — galaxies: haloes — cosmology: theory — cosmology: dark matter

1 INTRODUCTION

In the current Cold Dark Matter (CDM) paradigm, the hierarchical growth and buildup of dark matter haloes is the foundation on which galaxy formation and evolution unfolds itself. Hence, the understanding and characterization of the formation and properties of CDM haloes is a fundamental component of any theory of galaxy formation (see Mo et al. 2010 for a detailed overview).

The formation history of a dark matter halo is conveniently characterized by its merger tree, which describes how its progenitors merge and accrete over cosmic time. For a given cosmological model, such merger trees can be constructed either from N-body simulations or from Monte-Carlo realizations based on the extended Press-Schechter (EPS) formalism (Bond et al. 1991; Bower 1991; Lacey & Cole 1993). When tracing a merger tree back in time, each halo breaks up into progenitor haloes, which themselves break up into progenitors, etc. The most massive progenitor of a given descendant halo (or the progenitor that con-

tributes most mass to its descendant, see §2.3) is called its *main* progenitor, and the *main branch* of the merger tree is defined as the branch tracing the main progenitor of the main progenitor of the main progenitor, etc. The mass history, $M(z)$, along this main branch is called the *mass accretion history* (hereafter MAH)[‡], and plays a crucial role; it is the property that is most often used to define halo formation (or assembly) times (e.g., Lacey & Cole 1993; Nusser & Sheth 1999; van den Bosch 2002a; Neistein, van den Bosch & Dekel 2006; Li et al. 2007, 2008; Giocoli et al. 2007; Giocoli, Tormen & Sheth 2012), and it is strongly correlated with various structural properties of dark matter haloes, such as halo concentration (e.g., Wechsler et al. 2002; Zhao et al. 2003b, 2009; Tasitsiomi et al. 2004; Giocoli et al. 2012; Ludlow et al. 2013), and substructure abundance (e.g., Gao et al. 2004; van den Bosch, Tormen & Giocoli 2005; Giocoli et al. 2010; Yang et al. 2011; Jiang & van den Bosch 2014b). In addition, the time derivative of the MAH gives the mass growth rate, which is directly related

---

[*] E-mail: frank.vandenbosch@yale.edu
[†] NSF Astronomy & Astrophysics Postdoctoral Fellow

[‡] Also sometimes called the 'mass assembly history' or 'mass aggregation history'.

to the rate at which haloes accrete baryons from the cosmic web (e.g., van den Bosch 2002a; Neistein & Dekel 2008a,b; Genel et al. 2009; McBride, Fakhouri & Ma 2009; Fakhouri, Ma & Boylan-Kolchin 2010), which is why MAHs are often used as the backbone for modeling the formation of (disk) galaxies (e.g., Eisenstein & Loeb 1996; Avila-Reese, Firmani & Hernández 1998; Firmani & Avila-Reese 2000; van den Bosch 2001, 2002b; Dutton et al. 2007). In fact, many properties of present-day galaxies are expected to be tightly correlated with the MAH of their host halo, including their morphology (e.g., Kauffmann, White & Guiderdoni 1993; Baugh, Cole & Frenk 1996) and their star formation rate (e.g., Hearin & Watson 2013; Watson et al. 2014; Hearin, Watson & van den Bosch 2014).

Numerous studies have investigated the properties of MAHs in (Λ)CDM cosmologies, which have revealed a number of trends. Using high resolution N-body simulations, Zhao et al. (2003a,b) found that the MAHs typically consist of two distinct phases: an early phase of rapid mass growth, and a later phase of slow growth (see also Tasitsiomi et al. 2004; Li et al. 2007). The early, rapid growth phase is characterized by major mergers which keep the system from settling in virial equilibrium (e.g., Cohn & White 2005). During this period the halo continuously reconfigures its structure through violent relaxation and phase mixing, while deepening its potential well. For reasons that are not yet understood, the end-point of this process is a (now virialized) dark matter halo with an NFW density profile (Navarro, Frenk & White 1997) with a concentration parameter, $c \sim 4$ (see §2.1 below for a definition of c). During the subsequent slow growth phase the halo predominantly grows in mass due to minor mergers and the accretion of diffuse matter. This mainly adds matter to the outskirts, and therefore causes the halo concentration parameter to increase (e.g., Zhao et al. 2009).

van den Bosch (2002a; hereafter vdB02) used EPS merger trees and numerical simulations to show that the *average* MAHs (averaged over many haloes of given mass), follow a simple, universal profile that is characterized by two parameters that scale with halo mass and cosmology. In particular, more massive haloes were shown to assemble later, which gives rise to a decreasing concentration-mass relation, and which is a simple consequence of the fact that the mass variance of the CDM power spectrum decreases with increasing mass. The halo-to-halo variance of MAHs, even for haloes of fixed present-day mass, is large. It is responsible for the scatter in the concentration-mass relation (e.g., Wechsler et al. 2002), is one of the dominant sources of scatter in the Tully-Fisher relation (e.g., Eisenstein & Loeb 1996; van den Bosch 2000; Dutton et al. 2007), and is correlated with the halo's large scale environment (e.g., Sheth & Tormen 2004; Gao, Springel & White 2005; Harker et al. 2006; Maulbetsch et al. 2007).

Whereas the MAHs of dark matter haloes have received abundant attention in the literature, there has been surprisingly little focus on the buildup of dark matter potential wells. In particular, the central potential depth is an important property. As shown in §2.1, it is directly proportional to the halo's maximum circular velocity, V_{max}, which is often used as the halo parameter of choice in abundance matching (e.g., Trujillo-Gomez et al. 2011; Reddick et al. 2012; Hearin et al. 2013; Zentner, Hearin & van den Bosch 2014). This

suggests that V_{max} may be a better 'regulator' of galaxy formation than halo mass. This should not come as a surprise, given that feedback is a crucial ingredient of galaxy formation, and the efficiency of feedback processes to expel matter and metals depends on the escape speed, and hence the depth of the central potential well. V_{max} also has the advantage that it can be much more reliably and robustly measured than halo mass, both from simulations and in observational data. In addition, it is free from issues related to 'pseudo-evolution' (Diemand, Kuhlen & Madau 2007; Cuesta et al. 2008; Zemp 2013; Diemer, More & Kravtsov 2013; Diemer & Kravtsov 2014), and is defined without any ambiguity, unlike halo mass, for which multiple definitions are in use[§].

The main goal of this paper is to study the potential well growth histories (hereafter PWGHs) of CDM haloes, which we characterize as the temporal evolution of V_{max} of a halo's main progenitor. In particular, we aim to provide a 'recipe' to compute the average PWGH for a halo of any given mass in any (reasonable) cosmology. To do so, we use EPS-based merger trees combined with a model, introduced in Jiang & van den Bosch (2014b), that allows us to compute V_{max} for each progenitor halo along the tree. We test and calibrate our model using merger trees and PWGHs extracted from the Bolshoi simulation (Klypin, Trujillo-Gomez & Primack 2011), and show that the PWGH can be inferred from the MAH combined with a model for the concentration-mass-redshift relation of dark matter haloes. Unfortunately, previous fitting functions used to describe average or median halo MAHs are inadequate, in that they either use a different definition for the main progenitor, or they are only valid for a single cosmology. We instead provide a new, universal model, and demonstrate that the average (and median) MAHs of haloes of different mass and in different cosmologies are related via a simple time transformation that is motivated by insights gained from the EPS formalism (see also Neistein, Macció & Dekel 2010).

This paper is organized as follows. In §2 we give a brief overview of the basics of dark matter haloes, followed by descriptions of our semi-analytical model and of the numerical simulation used to calibrate and test the model. In §3 we present the MAHs and PWGHs of dark matter haloes obtained using our semi-analytical model, and compare them to results from the Bolshoi simulation and to predictions from the models by Zhao et al. (2009) and Giocoli et al. (2012). In §4 we present our new and improved universal model for the average and median MAHs of dark matter haloes. We show how it can be used to compute the corresponding PWGHs, and use it to derive a fully analytical model for the average mass accretion rates of dark matter haloes. We summarize our findings in §5.

2   METHODOLOGY

This section describes the numerical simulations and semi-analytical models used to study the Mass Accretion Histories (MAHs) and Potential Well Growth Histories (PWGHs) of

---

[§] to great frustration of most practitioners, who constantly have to convert one definition to another.

dark matter haloes. However, we start with a brief introduction of halo basics, outlining a number of definitions and notations.

2.1 Halo Basics and Notation

Throughout this paper dark matter haloes at redshift z are defined as spherical systems with a virial radius $r_{\rm vir}$ inside of which the average density is equal to $\Delta_{\rm vir}(z)\,\rho_{\rm crit}(z)$. Here $\rho_{\rm crit}(z) = 3H^2(z)/8\pi G$ is the critical density for closure, and is given by

$$\Delta_{\rm vir}(z) = 18\pi^2 + 82x - 39x^2 \qquad (1)$$

with $x = \Omega_{\rm m}(z) - 1$ (Bryan & Norman 1998). The (virial) mass of a dark matter halo is defined as the mass within the virial radius $r_{\rm vir}$ and indicated by M.

We also assume throughout that dark matter haloes follow an NFW density profile

$$\rho(r) = \rho_{\rm crit}\frac{\delta_{\rm char}}{(r/r_{\rm s})\,(1 + r/r_{\rm s})^2}\,. \qquad (2)$$

Here $r_{\rm s}$ is the scale radius, and

$$\delta_{\rm char} = \frac{\Delta_{\rm vir}}{3}\,\frac{c^3}{f(c)}\,, \qquad (3)$$

with $c = r_{\rm vir}/r_{\rm s}$ the halo concentration parameter, and

$$f(x) = \ln(1 + x) - \frac{x}{1 + x}\,. \qquad (4)$$

The maximum circular velocity of a NFW halo occurs at a radius $r_{\rm max} \simeq 2.16\,r_{\rm s}$, and is given by

$$V_{\rm max} = 0.465\,V_{\rm vir}\,\sqrt{\frac{c}{f(c)}}\,, \qquad (5)$$

where

$$V_{\rm vir} = 159.43\,{\rm km\,s^{-1}}\left(\frac{M}{10^{12}\,h^{-1}{\rm M_\odot}}\right)^{1/3}\left[\frac{H(z)}{H_0}\right]^{1/3}$$
$$\left[\frac{\Delta_{\rm vir}(z)}{178}\right]^{1/6}\,, \qquad (6)$$

is the virial velocity, defined as the circular velocity at the virial radius. The gravitational potential of a spherical NFW density distribution is given by

$$\Phi(r) = -V_{\rm vir}^2\,\frac{\ln(1 + cx)}{f(c)\,x} = -\left(\frac{V_{\rm max}}{0.465}\right)^2\frac{\ln(1 + cx)}{cx}\,, \qquad (7)$$

where $x = r/r_{\rm vir}$ is the radius normalized by the halo's virial radius. Using the Taylor series expansion for $\ln(1+x)/x$ we thus see that the central potential of an NFW halo is given by

$$\Phi_{\rm c} \equiv \Phi(r = 0) = -\left(\frac{V_{\rm max}}{0.465}\right)^2\,. \qquad (8)$$

Hence, the maximum circular velocity of an NFW halo is a *direct* measure of its central potential depth.

Throughout we use subscripts '0' to refer to the value at redshift z_0, which we normally take to be the present day (i.e., $z_0 = 0$), unless stated otherwise. We use time, t, and redshift, z, interchangeably as our 'time coordinate', and use $t_0 - t$ to indicate lookback time. Finally, given an ensemble $X = \{X_1, X_2, ...X_n\}$, we use $\langle X\rangle$ to indicate the ensemble's *average*, while $\langle X\rangle_{\rm med}$ is used to refer to its *median*.

Typically we will plot medians whenever we also display the halo-to-halo variance, and use averages when that is not the case.

2.2 Semi-Analytical Model

One of the main goals of this paper is to present a universal model for the MAHs and PWGHs of dark matter haloes as a function of halo mass and cosmology. We trace the assembly of dark matter haloes using a semi-analytical model based on merger trees constructed using the extended Press-Schechter (EPS) formalism (Bond et al. 1991), which provides the progenitor mass function (hereafter PMF), $n_{\rm EPS}(M_{\rm p}, z_1|M_0, z_0)\,{\rm d}M_{\rm p}$, that describes the average number of progenitors of mass $M_{\rm p} \pm {\rm d}M_{\rm p}/2$ that a descendant halo of mass M_0 at redshift z_0 has at redshift $z_1 > z_0$. Starting from some target host halo mass M_0 at z_0, one can use this PMF to draw a set of progenitor masses $M_{\rm p,1}, M_{\rm p,2}, ..., M_{\rm p,N}$ at some earlier time $z_1 = z_0 + \Delta z$, where $\sum_{i=1}^{N} M_{\rm p,i} = M_0$ in order to assure mass conservation. The time-step Δz used sets the 'temporal resolution' of the merger tree, and may vary along the tree. This procedure is then repeated for each progenitor with mass $M_{\rm p,i} > M_{\rm res}$, thus advancing 'upwards' along the tree. The minimum mass $M_{\rm res}$ sets the 'mass resolution' of the merger tree and is typically expressed as a fraction of the final host mass M_0.

We construct our merger trees using the method of Parkinson, Helly & Cole (2008; hereafter P08), which uses the 'binary method with accretion' of Cole et al. (2000) combined with a PMF that is tuned to match results from the Millennium Simulation (Springel et al. 2005), rather than the PMF that follows from EPS. In particular, progenitor halo masses are drawn from

$$n(M_{\rm p}, z_1|M_0, z_0) = n_{\rm EPS}(M_{\rm p}, z_1|M_0, z_0)\,G(M_{\rm p}, M_0, z_0)\,, \qquad (9)$$

where $G(M, M_0, z_0)$ is a perturbing function that is calibrated using merger trees extracted from the Millennium simulation by Cole et al. (2008), and which is given by

$$G(M, M_0, z_0) = 0.57\left[\frac{\sigma^2(M)}{\sigma^2(M_0)}\right]^{0.19}\left[\frac{\delta_{\rm c}(z_0)}{\sigma(M_0)}\right]^{-0.01}\,. \qquad (10)$$

Here $\delta_{\rm c}(z) = 1.686/D(z)$ is the initial overdensity required for spherical collapse at redshift z, extrapolated to the present time using linear theory, $\sigma^2(M)$ is the mass variance[¶], and $D(z)$ is the linear growth rate. As shown in Jiang & van den Bosch (2014a), the P08 method yields halo merger rates, mass accretion histories, and unevolved subhalo mass functions (i.e., the mass function of subhaloes at accretion) that are all in good agreement with numerical simulations. In addition, van den Bosch & Jiang (2014) have shown that it can also be used to predict accurate *evolved* subhalo mass functions. Most importantly, even though $G(M, M_0, z_0)$ was calibrated for the cosmology used to run the Millennium simulation, the aforementioned studies have shown that it yields equally accurate results for other ΛCDM cosmologies.

[¶] i.e., the variance in the linear fluctuation field when smoothed with a top-hat filter of size $R = (3M/4\pi\bar\rho)^{1/3}$ with $\bar\rho$ the comoving density of the background.
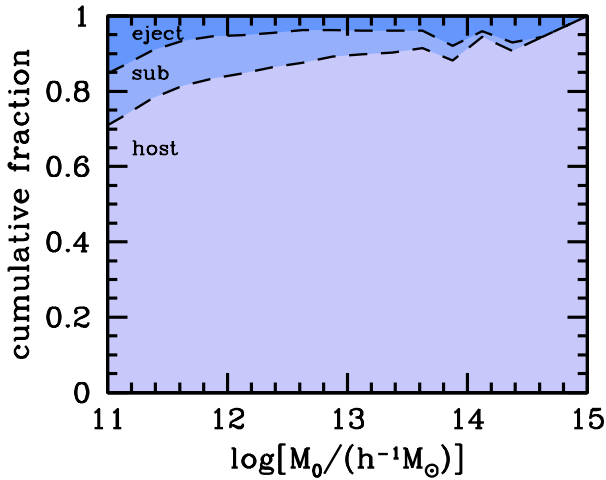
Figure 1. Cumulative fractions of host haloes, subhaloes and ejected haloes as function of halo mass in the Bolshoi simulation.

Throughout we always adopt a mass resolution of $M_{\rm res}/M_0 = 10^{-5}$ unless mentioned otherwise, and construct the merger trees using the time stepping advocated in Appendix A of P08 (which roughly corresponds to $\Delta z \sim 10^{-3}$; somewhat finer/coarser at high/low redshift). In order to speed up the code, and to reduce memory requirements, we down-sample the time resolution of each merger tree by registering progenitor haloes every time step $\Delta t = 0.1 t_{\rm ff}(z)^{\|}$. Here $t_{\rm ff}(z) \propto (1+z)^{-3/2}$ is the free-fall time for a halo with an overdensity of 200 at redshift z. Since the dynamical time of a halo is of order the free-fall time, there is little added value in resolving merger trees at higher time resolution than this. We have verified that indeed our results do not change if we register our merger trees using smaller time steps.

For a given merger tree, we determine the MAH by starting from the final host halo at $z = z_0$, and tracing the tree back in time, registering the mass of its main progenitor as function of redshift. Next we use this $M(z)$ to compute $V_{\rm max}(z)$ of the main progenitor as function of redshift, using the method of Jiang & van den Bosch (2014b). In brief, we assume that dark matter haloes follow NFW density profiles, for which $V_{\rm max}$ depends on the halo virial velocity and halo concentration as given by Eq. (5). It is well known that the concentration of a dark matter halo is strongly correlated with its MAH, in the sense that haloes that assemble earlier are more concentrated (e.g., Navarro et al. 1997; Wechsler et al. 2002; Ludlow et al. 2013). We use the model of Zhao et al. (2009), according to which halo concentrations are given by

$$c(M,t) = c(t, t_{0.04}) = 4.0 \left[1 + \left(\frac{t}{3.75\, t_{0.04}} \right)^{8.4} \right]^{1/8}, \quad (11)$$

(but see §3.3 below). Here $t_{0.04}$ is the proper time at which the host halo's main progenitor gained 4 percent of its mass M at proper time t, which we extract from the MAH. As shown in Jiang & van den Bosch (2014b) and van den Bosch & Jiang (2014), combining this methodology with

a simulation-based description for how $V_{\rm max}$ of a subhalo evolves as it experiences mass stripping, yields subhalo velocity functions, $dN/d\ln(V_{\rm max}/V_{\rm vir,0})$, that are in excellent agreement with simulation results. In what follows we refer to this semi-analytical model for computing the MAHs and PWGHs of dark matter haloes as 'MergerTrees',

2.3 Numerical Simulation

In order to test and, where needed calibrate, our semi-analytical model we use the Bolshoi simulation (Klypin et al. 2011), which follows the evolution of 2048^3 dark matter particles using the Adaptive Refinement Tree (ART) code (Kravtsov, Klypin & Khokhlov 1997) in a flat ΛCDM model with parameters $\Omega_{\rm m,0} = 1 - \Omega_{\Lambda,0} = 0.27$, $\Omega_{\rm b,0} = 0.0469$, $h = H_0/(100\,{\rm km\,s^{-1}\,Mpc^{-1}}) = 0.7$, $\sigma_8 = 0.82$ and $n_{\rm s} = 0.95$ (hereafter 'Bolshoi cosmology'). The box size of the Bolshoi simulation is $L_{\rm box} = 250 h^{-1}$ Mpc, resulting in a particle mass of $m_{\rm p} = 1.35 \times 10^8\, h^{-1} {\rm M}_\odot$.

We use the publicly available halo catalogs and merger trees[**] obtained using the phase-space halo finder ROCKSTAR (Behroozi et al. 2013a,b), which uses adaptive, hierarchical refinement of friends-of-friends groups in six phase-space dimensions and one time dimension. As demonstrated in Knebe et al. (2011, 2013), this results in a very robust tracking of (sub)haloes (see also van den Bosch & Jiang 2014). In line with the halo definition used throughout this paper, the ROCKSTAR haloes are defined as spheres with an average density equal to $\Delta_{\rm vir}\rho_{\rm crit}$. Details regarding the construction of the merger trees can be found in Behroozi et al. (2013b).

Throughout this paper we restrict ourselves to haloes that at $z = 0$ have accumulated a mass $M_0 \geq 10^{11}\, h^{-1}{\rm M}_\odot$ (corresponding to ≥ 740 particles per halo). Using the merger trees, we split the population of $z = 0$ haloes in three categories:

• host haloes; these are distinct haloes that are not, and never have been, located within the virial radius of another, more massive halo.
• subhaloes; these are haloes that at $z = 0$ are located within the virial radius of another, more massive halo.
• ejected haloes; these are haloes that at $z = 0$ are distinct, but whose main progenitor has at one or more occasions passed through the virial region of a more massive halo. Ejected haloes are also sometimes called 'backsplash' haloes.

Fig. 1 shows the cumulative fractions of these different categories as function of their mass at $z = 0$; host haloes clearly dominate, with a fraction that increases from ~ 70 percent for haloes with $M_0 = 10^{11}\, h^{-1}{\rm M}_\odot$ to 100 percent at the massive end. The remainder is split roughly equally between subhaloes and ejected haloes. These statistics are in good agreement with previous studies (e.g., Wang et al. 2009a).

For each host halo at $z = 0$ we use the merger trees to determine their MAH, $M(z)/M_0$, as well as their PWGH, $V_{\rm max}(z)/V_{\rm vir,0}$. It is important to point out that in simulations the definition of 'main progenitor' is not without ambiguity. Whereas some studies simply define it as the

---

$^{\|}$ For the Bolshoi cosmology considered here, this results in $N = 329$ time steps between $z = 50$ and $z = 0$.

** http://hipacc.ucsc.edu/Bolshoi/MergerTrees.html
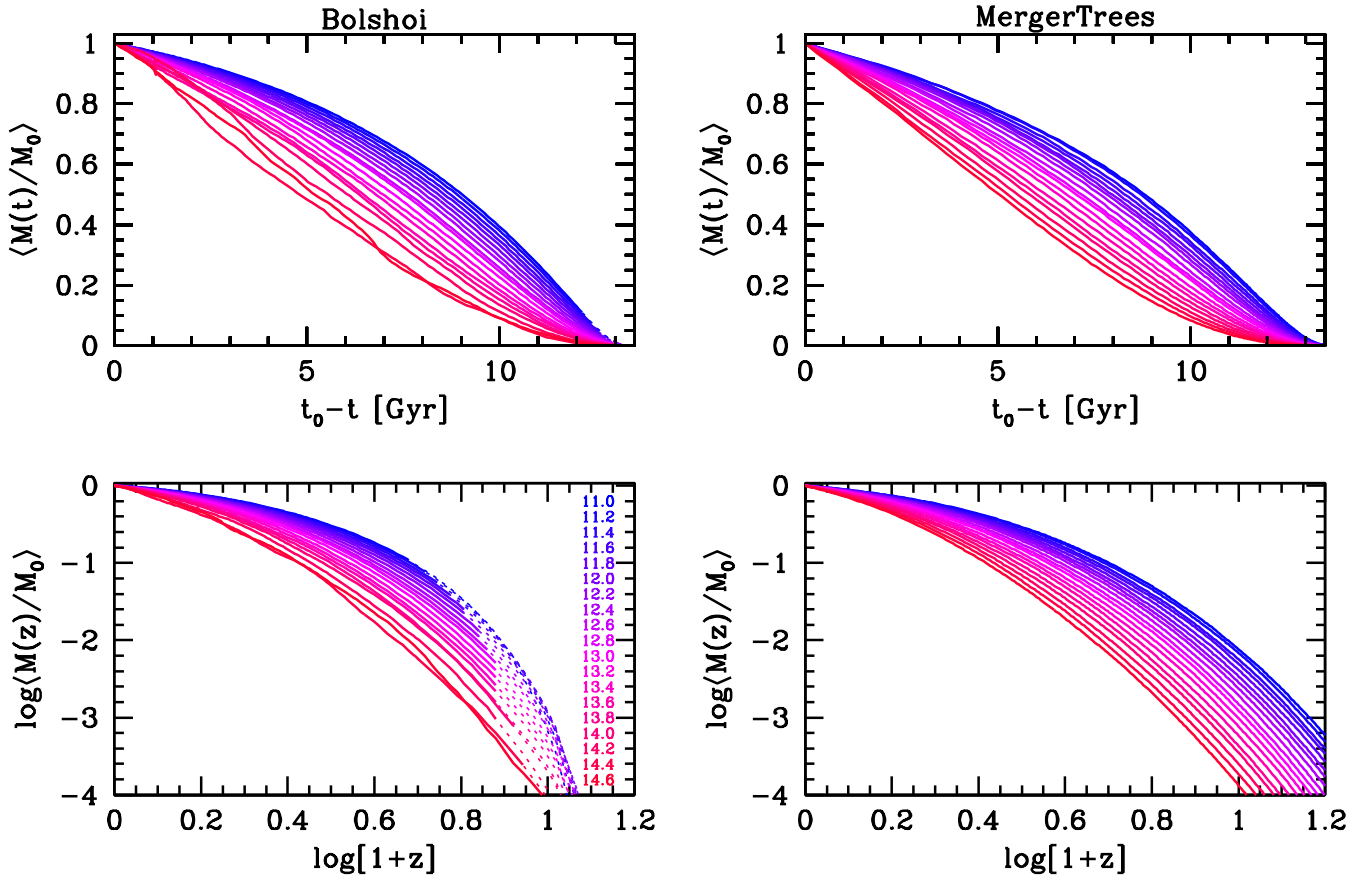
Figure 2. Average mass accretion histories for host haloes at $z = 0$. Different colors indicate different host halo masses, with the corresponding value for $\log[M_0/(h^{-1}\mathrm{M}_\odot)]$ indicated in the lower left-hand panel. Upper and lower panels plot $\langle M(t)/M_0\rangle$ as function of lookback time and $\log\langle M(z)/M_0\rangle$ as function of $\log[1+z]$, which accentuate the behaviors at late and early times, respectively. Panels on the left show the results obtained from the Bolshoi simulation, where each line is the average obtained from all haloes in a mass bin that is 0.2dex wide. Solid lines show the average MAHs over the range where the main progenitors of $> 90\%$ of all host haloes can be traced. Dotted lines are the extensions obtained taking the average over all host haloes. Panels on the right show the results from MergerTrees, where each average is obtained using 2000 realizations.

descendant's most massive progenitor (e.g., van den Bosch 2002; McBride et al. 2009; Fakhouri et al. 2010; Behroozi et al. 2013c; Behroozi & Silk 2014), others define it as the progenitor that contributes most mass to the descendant (e.g., Wechsler et al. 2002; Zhao et al. 2003a,b, 2009; Giocoli et al. 2012). In the EPS merger trees these two definitions are identical, but in numerical simulations this is not necessarily the case. For example, consider two progenitors of a descendant halo of mass M; progenitor A with mass $M_A = 0.53M$ and progenitor B with mass $M_B = 0.51M$. Suppose that B contributes its entire mass to its descendant, whereas A only contributes $0.49M$ (the remaining $0.04M$ ending up just outside the boundary of the descendant halo). In this case, A is the most massive progenitor, whereas B is the one that contributes most of its mass. In this paper, we use the publicly available merger trees from the Bolshoi simulation, and always define the main progenitor as the most massive one. Although we consider this the more preferable choice when comparing to EPS and when using MAHs in the framework of galaxy formation, we acknowledge that this somewhat ambiguous and that one can probably make equally strong arguments in favor of picking the most-contributing progenitor as the main progenitor. Although it is relatively

rare that the most-massive progenitor is different from the progenitor that provides most mass, the different definitions for main progenitor result in (average) MAHs that can be significantly different (see §3.2).

As demonstrated in Appendix A, the MAHs of subhaloes and ejected haloes are very different from those of host haloes. Since this paper focuses on the MAHs and PWGHs of host haloes, and since several studies have argued that galaxies that reside in ejected haloes have properties that are more reminiscent of satellite galaxies (those residing in subhaloes) than of central galaxies (e.g., Wang et al. 2009b; Geha et al. 2012; Wetzel et al. 2014), we remove both subhaloes and ejected haloes from our sample.

2.4 Why use a Semi-Analytical Model?

In an era in which numerical simulations have become common-place in astrophysical research, one may wonder why one would resort to semi-analytical techniques to study MAHs and/or PWGHs. In fact, there are a number of reasons why we believe this to be important, useful and even necessary.

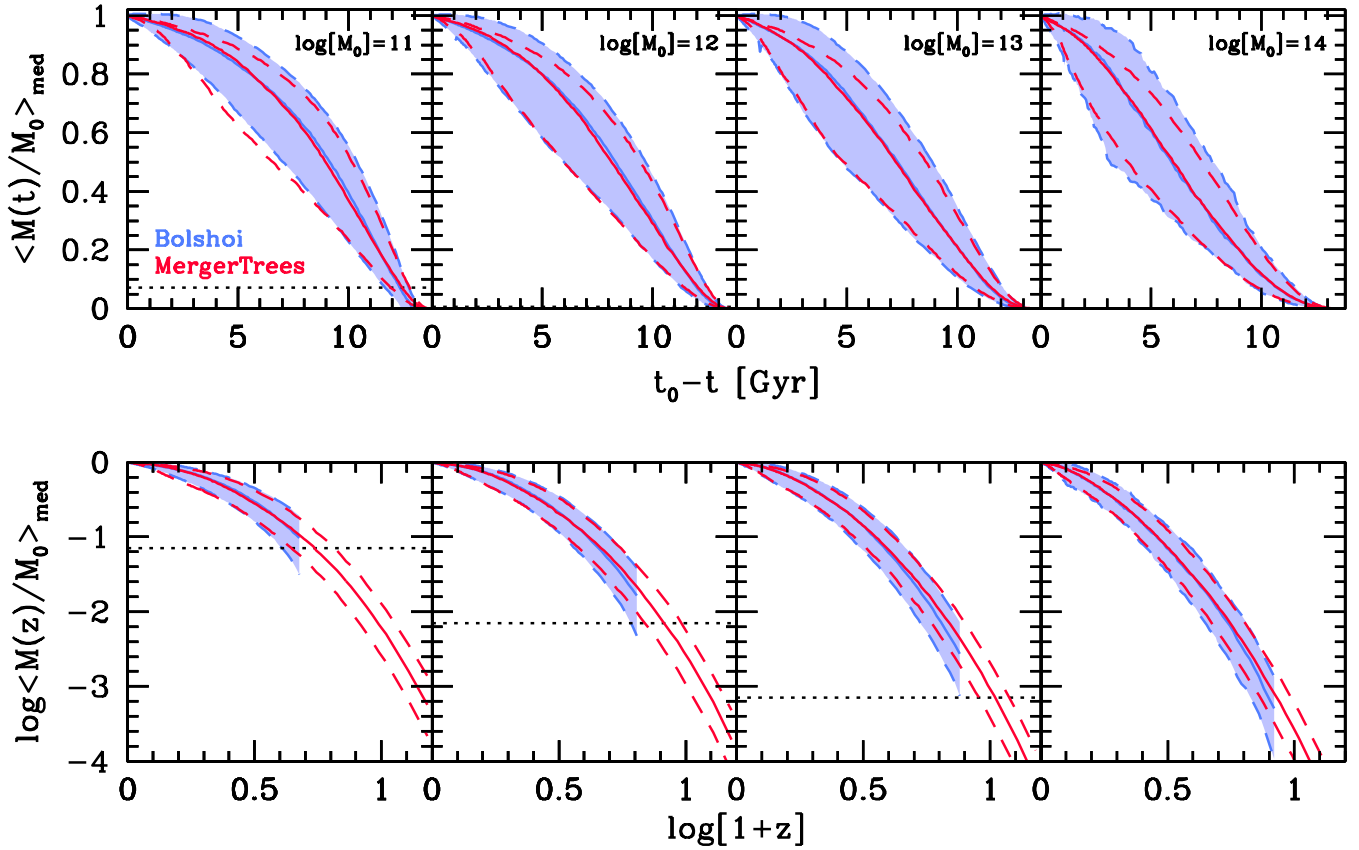The necessity comes mainly from the limited mass res-

Figure 3. Median mass accretion histories. Comparison of Bolshoi results (blue) with results obtained using MergerTrees (red). Results are shown for four different mass bins, as indicated in the upper left corner of the upper panels. Solid lines depict the medians while the dashed lines indicate the corresponding 16 and 84 percentiles (shaded in the case of Bolshoi). Note that the solid blue line is mostly invisible because the solid red line lies on top of it, indicating excellent agreement between simulations and MergerTrees. Horizontal dotted lines (in black) indicate where the mass of the main progenitor drops below $7 \times 10^9 \, h^{-1} \mathrm{M}_\odot$, which corresponds to 50 particles in the Bolshoi simulation, and roughly reflects the mass scale below which the simulation results are affected by resolution effects.

olution in numerical simulations: suppose we want to trace the main progenitor of a halo back in time to when its V_{max} was roughly 10 percent of the present day value. For a Milky-Way sized halo this implies resolving the main progenitor to when it roughly has a virial temperature of 10^4K. As we will see below, this requires resolving the main progenitor of a $z = 0$ halo of mass M down to the point where it drops below $10^{-4}M$. A reliable measurement of V_{max} of a simulated dark matter haloes requires that it is resolved with at least 100 particles, which therefore implies a particle mass $m_{\mathrm{p}} < 10^{-6}M$. Obtaining reliable statistics requires that the simulation volume contains at least of order 1000 such host haloes, which in turn implies a simulation volume $V > 1000/n(M)$, where $n(M) = \mathrm{d}N/\mathrm{d}\ln M$ is the halo mass function. Using that the total number of particles in the simulation box is $N_{\mathrm{p}} = \Omega_{\mathrm{m}} \rho_{\mathrm{crit}} V/m_{\mathrm{p}}$, we then find that we need

$$N_{\mathrm{p}} > 2.6 \times 10^{10} \left(\frac{\Omega_{\mathrm{m}}}{0.3} \right) \left[\frac{M \, n(M)}{10^{9.5} h^2 M_\odot \mathrm{Mpc}^{-3}} \right]^{-1} \qquad (12)$$

where we have used that in a ΛCDM cosmology, to good approximation, $M \, n(M) \sim 10^{9.5} h^2 M_\odot \mathrm{Mpc}^{-3}$ for present-day haloes with mass M below the characteristic mass M^*. For more massive haloes, the required number of particles increases exponentially. Hence, proper statistics of MAHs

(and PWGHs) that are well resolved down to $10^{-4}M$ requires simulations that are roughly three times the size of Millennium or Bolshoi, which are among the largest simulations that have been run to date. Although it is not infeasible that such simulations will be run in the not too distant future, the computational costs will be enormous. This is especially true in comparison to the analytical models, which can construct thousands of merger trees in a matter of minutes or hours (depending on the mass resolution used). Hence, it is clear that there is great virtue in having a reliable, well calibrated semi-analytical model, especially if it can be used for different cosmologies.

In addition, by resorting to simplified prescriptions of the underlying dynamics, semi-analytical models are extremely useful for gaining insight and understanding. Furthermore, although the accuracy of a numerical simulation is only limited by its mass and force resolution, there are non-trivial difficulties involved in identifying haloes and in linking them to their earlier progenitors. As a result, depending on the algorithms used, one can obtain merger trees that differ substantially, even when applied to the same simulation (e.g. Helly et al. 2003; Harker et al. 2006; Cole et al. 2008; Fakhouri & Ma 2008; Genel et al. 2008, 2009; Fakhouri, Ma & Boylan-Kolchin 2010; Srisawat et al. 2013). This is a problem that will be difficult to overcome, and implies
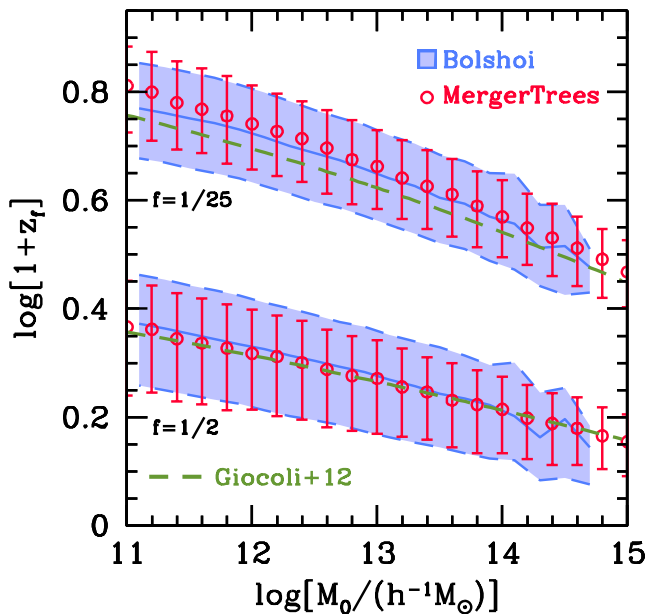
Figure 4. Halo formation redshifts, z_f, as function of halo mass, M_0, for two values of f, as indicated. The solid blue line indicates the median in the Bolshoi simulation, with the shaded region, bounded by two dashed curves, indicating the 68 percent confidence intervals. Red, open circles are the median formation redshifts obtained with MergerTrees while the errorbars reflect the 68 percent range. Green, dashed lines are the model predictions of Giocoli et al. (2012), and are shown for comparison. Note the excellent agreement between MergerTrees and simulation results.

that merger trees extracted from numerical simulations have their own shortcomings and are not always completely reliable. Hence, it is important and useful to have some alternatives in the form of a semi-analytical model.

3 RESULTS

3.1 Mass Accretion Histories

Fig. 2 plots the *average* MAHs for haloes of different masses (different colors). We plot both $\langle M(t)/M_0\rangle$ as function of lookback time (upper panels), as well as $\log\langle M(z)/M_0\rangle$ as function of $\log[1+z]$ (lower panels). These accentuate the behavior of the MAHs at late and early times, respectively. Panels on the left show the results obtained from the Bolshoi simulation, where each line is the average obtained from all haloes in a mass bin that is 0.2dex wide. Because of the limited mass resolution, the MAHs become incomplete at early-times, when the main progenitor mass drops below the mass resolution limit. Following Zhao et al. (2009), we therefore only plot (as solid lines) the average MAHs up to the redshift or lookback time where the progenitors of $>90\%$ of all host haloes in consideration can be traced (i.e., where more than 90% of all host haloes have a main progenitor that is still resolved in the Bolshoi simulation). Dotted lines are the extensions one obtains when taking the average over all host haloes, assuming a main progenitor mass of zero whenever the MAH drops below the resolution limit. The number of haloes used in the ensemble averages ranges from 145126 for the mass bin with $\log[M_0/(h^{-1}\mathrm{M}_\odot)]\in[10.9,11.1]$

to a meager 22 for the $[14.5,14.7]$-bin, which explains the increasing 'jaggedness' of the average MAHs with increasing halo mass. The panels on the right show the results from our semi-analytical model 'MergerTrees', where each curve is obtained by taking the average of 2000 MAHs for a host halo with a mass equal to the midpoint of the logarithmic mass bin[††] ; i.e., for the bin $\log[M_0/(h^{-1}\mathrm{M}_\odot)]\in[10.9,11.1]$ this implies a halo mass of $M_0=10^{11}\,h^{-1}\mathrm{M}_\odot$.

A few trends are apparent. First of all, it is clear that more massive haloes assemble their mass later, consistent with hierarchical structure formation and with numerous previous findings (e.g., vdB02; Maulbetsch et al. 2007; Zhao et al. 2009; Fakhouri et al. 2010; Yang et al. 2011; Giocoli et al. 2012). Secondly, overall the simulation and MergerTrees results are in good, qualitative agreement, at least over the range where $>90\%$ of the MAHs are resolved (i.e., are represented by solid, rather than dotted lines). Fig. 3 shows a more direct comparison, this time of the *median* MAHs in the Bolshoi simulation (blue) and those obtained using MergerTrees (red). Solid and dashed lines indicate the median and the 68 percentile intervals, while the horizontal dotted lines indicate the mass scale where $M(z)$ drops below $7\times10^9\,h^{-1}\mathrm{M}_\odot$. This corresponds to 50 particles per halo, and roughly reflects the mass scale below which the Bolshoi simulation results become strongly affected by resolution effects. Overall, the median results obtained from MergerTrees are in excellent agreement with the simulation results. Even the 68 percentile intervals are in good agreement, although the simulation results reveal a more pronounced tail towards higher $M(t)/M_0$ at late times (i.e., for lookback times $t\lesssim5\mathrm{Gyr}$). This discrepancy is larger for more massive host haloes and likely reflects subtle issues related to ejected haloes. For example, consider a halo of mass M_1 that at time t_1 accreted another halo of mass $M_2\lesssim M_1$. If M_2's orbital trajectory places it outside of the virial radius of M_1 at the present day then, in the simulation, halo M_2 is considered an ejected halo (and thus removed from the sample), while M_1 is found to not have grown in mass since time t_1. In our semi-analytical model, however, no (sub)halo is ever ejected; hence, M_1 is considered to have grown in mass from M_1 to M_1+M_2 since time t_1. Hence, MergerTrees will have a smaller fraction of haloes that have experienced little recent growth than what is seen in simulations.

As a final comparison, Fig. 4 plots different halo assembly redshifts, z_f, defined as the redshift at which the main progenitor of a halo of mass M_0 at $z=0$ first reaches a mass fM_0. Results are shown for $f=0.5$ and $f=0.04$, as indicated. The agreement between simulations (blue) and MergerTrees (red) is excellent, both in terms of the medians and the 68 percentile intervals. For comparison, the green, solid lines are the model prediction of Giocoli et al. (2012): these are in excellent agreement for $f=0.5$, but somewhat underpredict the $z_{0.04}$ compared to the results from both MergerTrees and the Bolshoi simulation. Most likely this is a manifestation of the fact that Giocoli et al. (2012) define the main progenitor as the most-contributing progen-

[††] We have verified that drawing the 2000 halo masses from the full mass bin as sampled by the halo mass function yields results that are indistinguishable.
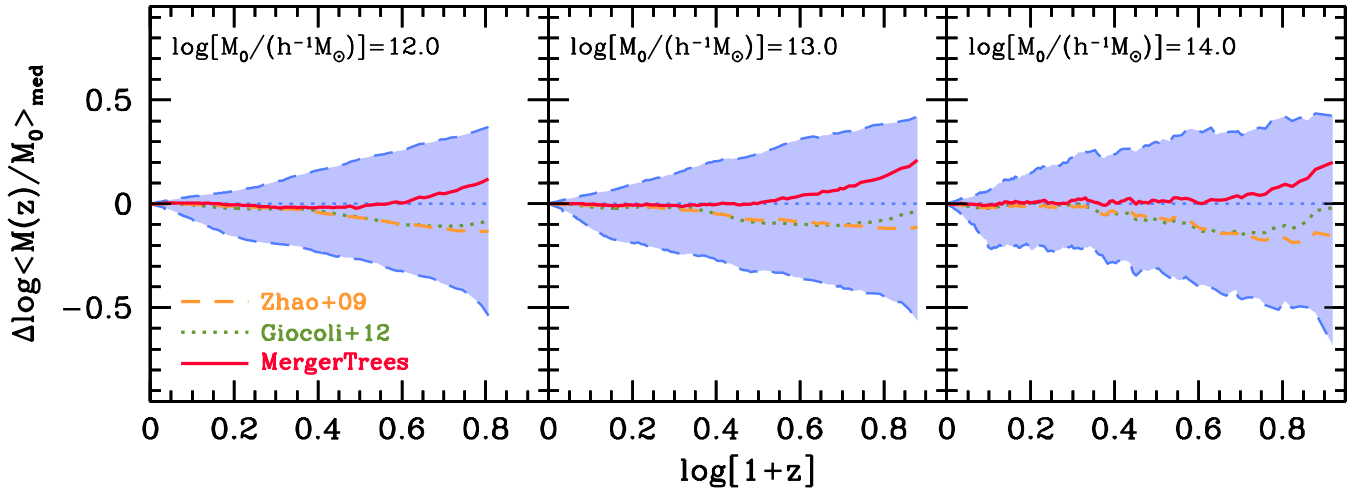
Figure 5. The differences $\Delta \log \langle M(z)/M_0 \rangle_{\mathrm{med}}$ between the median MAH obtained from the Bolshoi simulation and MergerTrees (red, solid lines), the universal model of Zhao et al. (2009; orange, dashed lines), and the universal model of Giocoli et al. (2012; green, dotted lines). Results are shown for three halo masses as indicated, while the shaded region indicates the 68 percentile interval. See text for discussion.

itor, whereas we define it to be the most-massive one (see §2.3).

3.2 Comparison with Previous Studies

As mentioned in §1, a number of studies have already investigated the MAHs of CDM haloes. Here we briefly describe some of the most relevant studies, and contrast their findings with those presented here.

First, it is important to distinguish between two different kinds of studies. On the one hand there are numerous studies that presented fitting functions for the average and/or median MAHs (or their time-derivatives) based on one particular numerical simulation (e.g., Neistein & Dekel 2008a; McBride et al. 2009; Genel et al. 2009; Fakhouri et al. 2010; Wu et al. 2013). These are only of limited use, as they are only valid for the particular cosmology adopted in that simulation. Even though most cosmological parameters are fairly well constrained these days, the remaining uncertainties translate into relatively large differences for the MAHs and PWGHs (see Appendix B). As a consequence, these studies can not be used for a meaningful comparison with the results from the Bolshoi simulation presented here.

In this section we therefore only focus on studies that have presented a universal model for the MAHs of dark matter haloes as function of halo mass, redshift and cosmology, and which can therefore be used to predict the average or median MAHs of haloes in the Bolshoi cosmology. The first such study was that by vdB02, who used EPS merger trees to investigate how the *average* MAH scales with halo mass and cosmology. However, those merger trees were constructed using the method developed by Somerville & Kolatt (1999), which has since been shown to yield MAHs that are systematically biased with respect to simulation results (e.g., Zhang, Ma & Fakhouri 2008; Jiang & van den Bosch 2014a). Indeed, we find the 'universal function' of vdB02 to be a poor fit to the average MAHs in the Bolshoi simulation, and will not consider it further. More recently, Zhao et al. (2009; hereafter Z09) used some elements from EPS theory to de-

velop a universal model for the MAHs of dark matter haloes, which they calibrated using a large suite of numerical simulations for different cosmologies. A similar approach was taken by Giocoli et al. (2012; hereafter G12), who derived a method for computing the median MAHs that yield results that are very similar to Zhao et al. , but using a prescription that is easier to implement (see also Giocoli et al. 2013, where the same method was extended to non-standard, coupled dark energy cosmologies). Unfortunately, both Z09 and G12 defined their main progenitor as the most-contributing one, which has to be taken into account when comparing their results to ours.

Fig. 5 compares the predictions of the Z09 and G12 models with the median MAHs in the Bolshoi simulation and with those obtained using MergerTrees. All model predictions are made for the Bolshoi cosmology. Plotted are the differences, $\Delta \log \langle M(z)/M_0 \rangle_{\mathrm{med}}$, with respect to the median MAH of haloes in the Bolshoi simulation. The shaded region, bounded by the two blue, dashed curves, indicates the 68 percent halo-to-halo variance in the Bolshoi simulation, while the red, orange and green lines are the model predictions from MergerTrees, Z09 and G12, respectively. They all agree with each other and with the Bolshoi simulation results for $z \lesssim 1.5$. At higher redshifts, the model predictions of Z09 and G12 both start to underpredict $\langle M(z)/M_0 \rangle_{\mathrm{med}}$. Most likely this is a manifestation of the different methods used to define the main progenitor, which is expected to yield MAHs that diverge with increasing redshift. Although the effect is small compared to the halo-to-halo variance, it is clear that one cannot use the universal models of Z09 and/or G12 to describe the median MAHs obtained with MergerTrees or obtained from simulations when the main progenitor is defined to be the most-massive one. In §4 we therefore present a new, universal model that is easy to use, and that is valid for the main-progenitor definition adopted here.

Finally, Fig. 5 demonstrates that MergerTrees yields MAHs that are in good agreement with the Bolshoi simulation results out to $z \sim 3$, but then start to overpredict
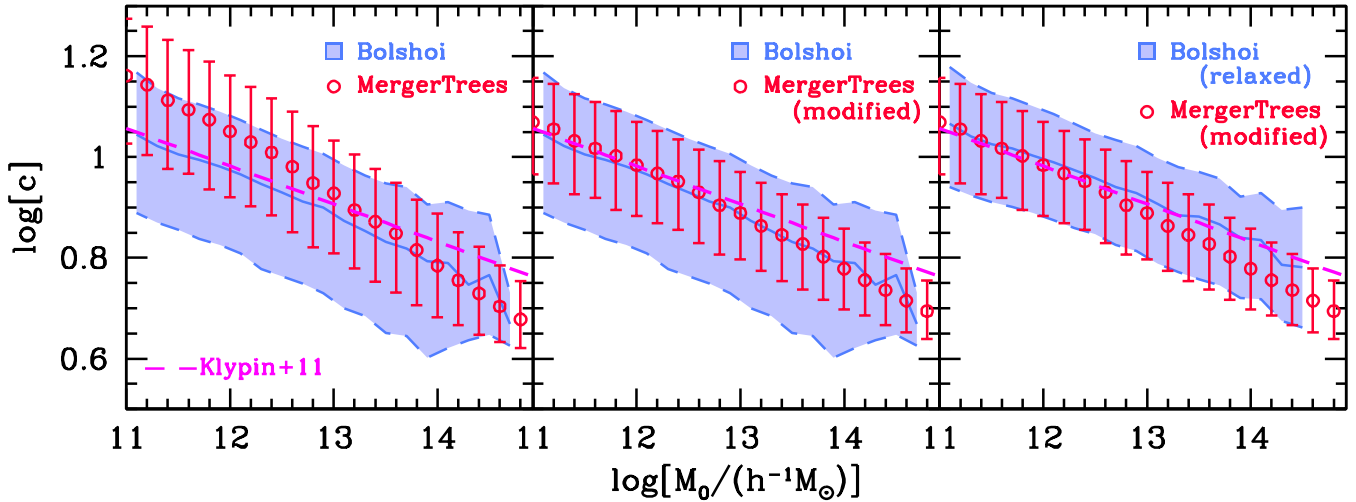
Figure 6. Concentration mass relations. The solid and dashed blue curves indicate the median and the 16 and 84 percentiles of the halo concentrations in the Bolshoi simulation. Red, open circles indicate the medians obtained using MergerTrees, with the errorbars reflecting the 68 percent interval. The dashed, magenta line is the median concentration-mass relation obtained from the Bolshoi simulation by Klypin et al. (2011), and is shown for comparison. In the left-hand panel, all host haloes in the Bolshoi simulation have been used, and concentrations in MergerTrees have been obtained using Eq. (11). In the middle panel, the Bolshoi data is the same, but this time concentrations in MergerTrees are computed using Eq. (14). Finally, in the right-hand panel only the relaxed haloes in the Bolshoi simulation are used (see text for definition), while the MergerTrees results are the same as in the middle panel.

$\langle M(z)/M_0 \rangle_{\rm med}$. Note, though, that this discrepancy sets in close to the mass resolution limit of the simulation (cf. dotted curves in lower panels of Fig. 3). Hence, it remains to be seen whether it reflects a true shortcoming of MergerTrees or whether it is merely a manifestation of limited mass resolution in the Bolshoi simulation.

3.3 Halo Concentrations

The main goal of this paper is to study the potential well growth histories, $V_{\rm max}(t)/V_{\rm vir,0}$, of dark matter haloes. Under the assumption that dark matter haloes have NFW density profiles, the maximum circular velocity, $V_{\rm max}$, is uniquely specified by the halo's mass, M, and concentration, c (see §2.1). As demonstrated in §3.1 above, MergerTrees accurately describes the halo mass assembly history. Hence, it is to be expected that it will also yield accurate PWGHs as long as it can accurately predict halo concentrations.

In our model, halo concentrations are computed using the model of Zhao et al. (2009), given by Eq. (11), which links halo concentration to $t_{0.04}$, the cosmic time at which the halo's main progenitor first reaches a mass $0.04M_0$. As shown in Fig. 4, the $t_{0.04}$ obtained from MergerTrees are in excellent agreement with those obtained from the Bolshoi simulation. Hence, if the Z09 model is accurate, the halo concentrations predicted by MergerTrees should also be in good agreement with those obtained from the Bolshoi simulation.

The solid, blue line in Fig. 6 shows the *median* concentration-mass relation for $z = 0$ dark matter haloes in the Bolshoi simulation, while the blue shaded region indicates the 68 percentile interval. These concentrations have been obtained using the method of Klypin et al. (2011), i.e., they are inferred from $V_{\rm max}$ and M under the assumption that haloes follow an NFW profile, without having to ac-

tually fit the halo's density profile[‡‡]. For comparison, the magenta line corresponds to

$$c = 9.60 \left(\frac{M_0}{10^{12} \ h^{-1}{\rm M}_\odot} \right)^{-0.075} \qquad (13)$$

which is the median $z = 0$ concentration-mass relation obtained from the same Bolshoi simulation by Klypin et al. (2011). Although both results agree at the low mass end, the concentration-mass relation of Klypin et al. is somewhat shallower than that inferred here. We emphasize, though, that Klypin et al. used the Bounded-Density-Maxima (BDM) halo finder of Klypin & Holzman (1997), whereas the results presented here are based on ROCKSTAR. Since different halo finders assign slightly different masses to identical haloes (e.g., Knebe et al. 2011), this is most likely the cause of the small discrepancy seen at the massive end.

The red, open circles with errorbars in the left-hand panel of Fig. 6 are the median and 68 percentile intervals obtained from MergerTrees, using 2000 Monte Carlo realizations per halo mass bin. Although the median is in good agreement with the simulation results for $M_0 \gtrsim 5 \times 10^{13} \ h^{-1}{\rm M}_\odot$, it is systematically offset to larger concentrations for less massive haloes. The origin of this discrepancy most likely results from the fact that Zhao et al. (2009) calibrated their model using values for $t_{0.04}$ that are obtained from MAHs in which the main progenitor is defined to the most-contributing one, as opposed to the most-massive one. As is evident from Fig. 4 these different definitions result in different values for $t_{0.04}$, and thus in different predictions for the halo concentrations. Since it is prudent for estimating reliable $V_{\rm max}$ that our halo concentrations are

---

[‡‡] We have compared these to the concentrations obtain by fitting the actual halo density profiles and find results that are almost indistinguishable.

accurate, we modify Eq. (11) so that we reproduce the median concentration-mass relation in the Bolshoi simulation. The red circles with errorbars in the middle panel of Fig. 6 show the results obtained from MergerTrees if we assign halo concentrations using

$$c(t, t_{0.04}) = 4.0 \left[1 + \left(\frac{t}{3.40 \, t_{0.04}} \right)^{6.5} \right]^{1/8} . \qquad (14)$$

instead of Eq. (11). As is apparent, this modified model yields median halo concentrations that are in excellent agreement with the Bolshoi results. In what follows we will adopt this modified model throughout.

Although the median of the modified model is in excellent agreement with the simulation results, it predicts significantly less scatter. In particular, the simulations reveal concentration distributions at fixed mass, $\mathcal{P}(c|M)$, that have an extended tail towards lower concentrations. Such a tail is not present in the PDFs obtained using MergerTrees, which instead are close to log-normal. Several studies have shown that a low-concentration tail in $\mathcal{P}(c|M)$ is due to non-relaxed haloes, which are haloes that are temporarily out of virial equilibrium due to merger activity, and therefore poorly described by an NFW profile (e.g., Macciò et al. 2007, 2008; Neto et al. 2007; Ludlow et al. 2013). To test this, the blue shaded region in the right-hand panel indicates the 68 percentile interval obtained using only *relaxed* haloes in the Bolshoi simulation. Following Ludlow et al. (2013), these are defined as haloes for which the ratio of kinetic to potential energy, $T/|U| < 0.0625$, and the distance between halo barycenter and the location of the potential minimum is less than 7 percent of the virial radius. Roughly 84% of the Bolshoi haloes in the mass range $10^{11} \, h^{-1} \mathrm{M}_\odot \le \mathrm{M}_0 \le 10^{15} \, h^{-1} \mathrm{M}_\odot$ meet these criteria, and their $\mathcal{P}(c|M)$ is consistent with a log-normal with a scatter $\sigma_{\log c} \simeq 0.11$. Note that MergerTrees somewhat underpredicts the median concentration of relaxed haloes at the massive end, and that it also predicts that the amount of scatter decreases with increasing mass, from $\sigma_{\log c} \simeq 0.10$ for $M_0 = 10^{11} \, h^{-1} \mathrm{M}_\odot$ to 0.05 for $M_0 = 10^{15} \, h^{-1} \mathrm{M}_\odot$. Although the latter is not apparent in the Bolshoi simulations, it is in excellent agreement with Neto et al. (2007), who, using the Millennium simulation, found that *relaxed haloes* have log-normal distributions of halo concentration with a scatter that decreases from $\sigma_{\log c} = 0.11$ for $M_0 \sim 10^{12} \, h^{-1} \mathrm{M}_\odot$ to 0.06 for $10^{15} \, h^{-1} \mathrm{M}_\odot$. The origin of this discrepancy between the results of Neto et al. (2007) and that of the Bolshoi simulation presented here is unclear.

We conclude that our semi-analytical model with the modified $c(t, t_{0.04})$ relation of Eq. (14) yields a median concentration-mass relation that is in good agreement with the Bolshoi simulation, but with a scatter that is somewhat too small. Consequently, our model will also somewhat underestimate the halo-to-halo variance in PWGHs. An alternative would be to remove the unrelaxed haloes from the sample of simulated haloes, which is the approach that was taken by Ludlow et al. (2013). However, this would remove the ~ 15 percent of the haloes that experienced most growth in the recent past, and would therefore seriously bias the median and average results. Since (recent) merging is an essential ingredient of the CDM paradigm, we want our semi-analytical model to be representative of the entire popula-

tion of host haloes, not only of the subset of relaxed host haloes. As we demonstrate in the next section, our model accurately reproduces the median PWGHs of Bolshoi host haloes (including the unrelaxed ones), and only marginally underestimates the halo-to-halo variance.

3.4   Potential Well Growth Histories

Fig. 7 plots the *average* PWGHs for different bins in host halo mass (different colors). Results are shown for both the Bolshoi simulation (left-hand panels) and for MergerTrees (right-hand panels). Similar to Fig. 2, upper and lower panels plot the results linearly and logarithmically to better accentuate the behavior at late and early times, respectively. As before, solid lines indicate the results up to the redshift or lookback time where the progenitors of $> 90\%$ of all host haloes in consideration can be traced, while dotted lines show the extensions obtained averaging over all host haloes while assuming $V_{\max} = 0$ whenever the MAH drops below the resolution limit. Qualitatively, the simulation and MergerTrees results are in good agreement, at least over the range where $> 90\%$ of the MAHs are resolved (i.e., are represented by solid, rather than dotted lines).

Note that, contrary to the MAHs shown in Fig. 2, the PWGHs do not all converge to unity at $z = 0$. Rather, because of the concentration-mass relation, the present-day ratio of $V_{\max}/V_{\rm vir}$ is larger for more concentrated (less massive) haloes. Alternatively, we could have opted to define the PWGHs as $V_{\max}(t)/V_{\max,0}$, rather than $V_{\max}(t)/V_{\rm vir,0}$. However the former contains less information as it is trivially recovered from the latter by multiplying by $V_{\rm vir,0}/V_{\max,0}$ (i.e., dividing by the PWGH at $z = 0$.).

It is clear from Fig. 7 that less massive haloes establish their central potential wells earlier, and that this rank-order is preserved at all times; i.e., at any given time the main progenitor of what ends up being a less massive halo at $z = 0$ has already build up a larger fraction of its final, central potential well. Note that this rank-order-preservation is violated by the dotted curves in the left-hand panels, which stresses the importance of only averaging results over ensembles that are well resolved. Upon comparing Figs. 2 and 7, it is evident that dark matter haloes establish their potential wells before they have accreted a major fraction of their mass (see also Li et al. 2007 and Boylan-Kolchin et al. 2010). This behavior is especially evident from Fig. 8, which plots $\langle V_{\max}(t)/V_{\max,0} \rangle$ as function of $\langle M(t)/M_0 \rangle$. Colored lines are the averages obtained using MergerTrees for different halo masses (as indicated), while the blue dots indicate the averages obtained from the Bolshoi simulation for haloes with $12.9 < \log[M_0/(\, h^{-1} \mathrm{M}_\odot)] \le 13.1$. Errorbars indicate the 68 percent confidence interval of the Bolshoi haloes, and indicate that the halo-to-halo variance in this plot is small. Moreover, the MergerTrees results show that there is only a weak dependence on halo mass, so that the vast majority of all dark matter haloes will lie along the colored band. The reason why this relation is so tight is easy to understand from the fact that

$$\frac{V_{\max}(t)}{V_{\max,0}} = \frac{V_{\max}(t)}{V_{\rm vir}(t)} \frac{V_{\rm vir}(t)}{V_{\rm vir,0}} \frac{V_{\rm vir,0}}{V_{\max,0}}$$

$$= \frac{f(c)}{f(c_0)} \left[\frac{M(t)}{M_0} \right]^{1/3} \left[\frac{\Delta_{\rm vir}(t)}{\Delta_{\rm vir,0}} \right]^{1/6} \left[\frac{H(t)}{H_0} \right]^{1/3} , \qquad (15)$$
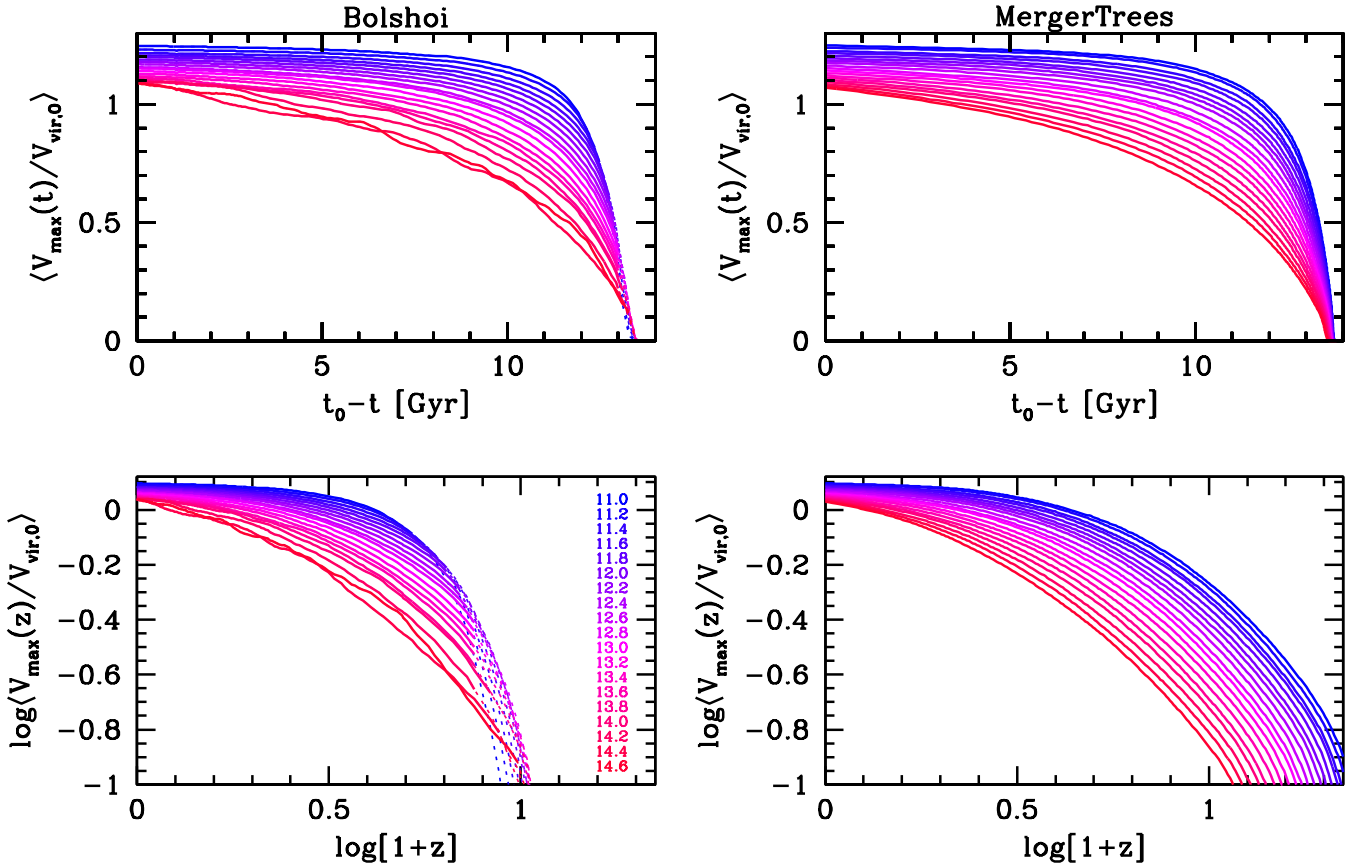
Figure 7. Same as Fig. 2, but for the average PWGHs, $V_{\mathrm{max}}(t)/V_{\mathrm{vir},0}$.

where c and c_0 are the halo concentrations corresponding to $M(t)$ and M_0, respectively, and we have used Eqs. (5)–(6). This shows that, to first order, $V_{\mathrm{max}}(t)/V_{\mathrm{max},0} \propto [M(t)/M_0]^{1/3}$. Deviations from this simple power-law reflect the concentration-mass-redshift relation of dark matter haloes and the fact that the virial overdensity and the Universe's expansion rate depend on redshift, but these dependencies are relatively weak. As a rule of thumb, the maximum circular velocity of a halo's main progenitor is already half the present day value by the time it has accreted only about 2 percent of its final mass. In addition, when the halo has assembled half its mass, its V_{max} is already at about 90 percent of its final value. More accurate results can be obtained using the universal model presented in §4 below.

Fig. 9 shows a more direct comparison of the *median* PWGHs in the Bolshoi simulation (blue) and those obtained using MergerTrees (red). As in Fig. 7, upper and lower panels plot the linear and logarithmic PWGHs, respectively. Solid and dashed lines indicate the median and the 68 percentile intervals. Except where the results drop below the mass resolution limit, the median results obtained from MergerTrees are in excellent agreement with the simulation results. Note that MergerTrees also predicts 68 percentile intervals that are in extremely good agreement with Bolshoi, even though it underpredicts the amount of scatter in the halo concentrations. Finally, the dotted, red lines show the results obtained from MergerTrees with the original concentration-mass-redshift relation of Zhao et al. (2009; Eq. [11]). As you can see, this somewhat overshoots V_{max} of

low mass haloes at late times, simply because it overpredicts their concentrations (see §3.3).

4 UNIVERSAL MODEL

Having demonstrated that our semi-analytical model can successfully reproduce the MAHs and PWGHs in the Bolshoi simulation, we now use it to develop a 'universal model' that can be used to quickly compute the average or median MAH and PWGH of a dark matter halo of any given mass and for any (realistic) ΛCDM cosmology, without having to run a numerical simulation or a set of halo merger trees.

The first step is to realize that once we have a model for the MAH, it is straightforward to compute the corresponding PWGH using

$$\frac{V_{\mathrm{max}}(t)}{V_{\mathrm{vir},0}} = \frac{V_{\mathrm{max}}(t)}{V_{\mathrm{vir}}(t)}\frac{V_{\mathrm{vir}}(t)}{V_{\mathrm{vir},0}}$$

$$= 0.465\, f(c) \left[\frac{M(t)}{M_0}\right]^{1/3} \left[\frac{\Delta_{\mathrm{vir}}(t)}{\Delta_{\mathrm{vir},0}}\right]^{1/6} \left[\frac{H(t)}{H_0}\right]^{1/3} \quad (16)$$

where c is the concentration of the main progenitor of mass M at time t (cf. Eq. [15]). Hence, the PWGH follows directly from the MAH and a model for the concentration-mass-redshift relation. In fact, the halo concentration can be computed directly from the MAH using Eq. (14), so that all we really need is a model for the MAH.

Unfortunately, as discussed in §3.2, the 'universal models' for the MAHs of dark matter haloes developed by Zhao
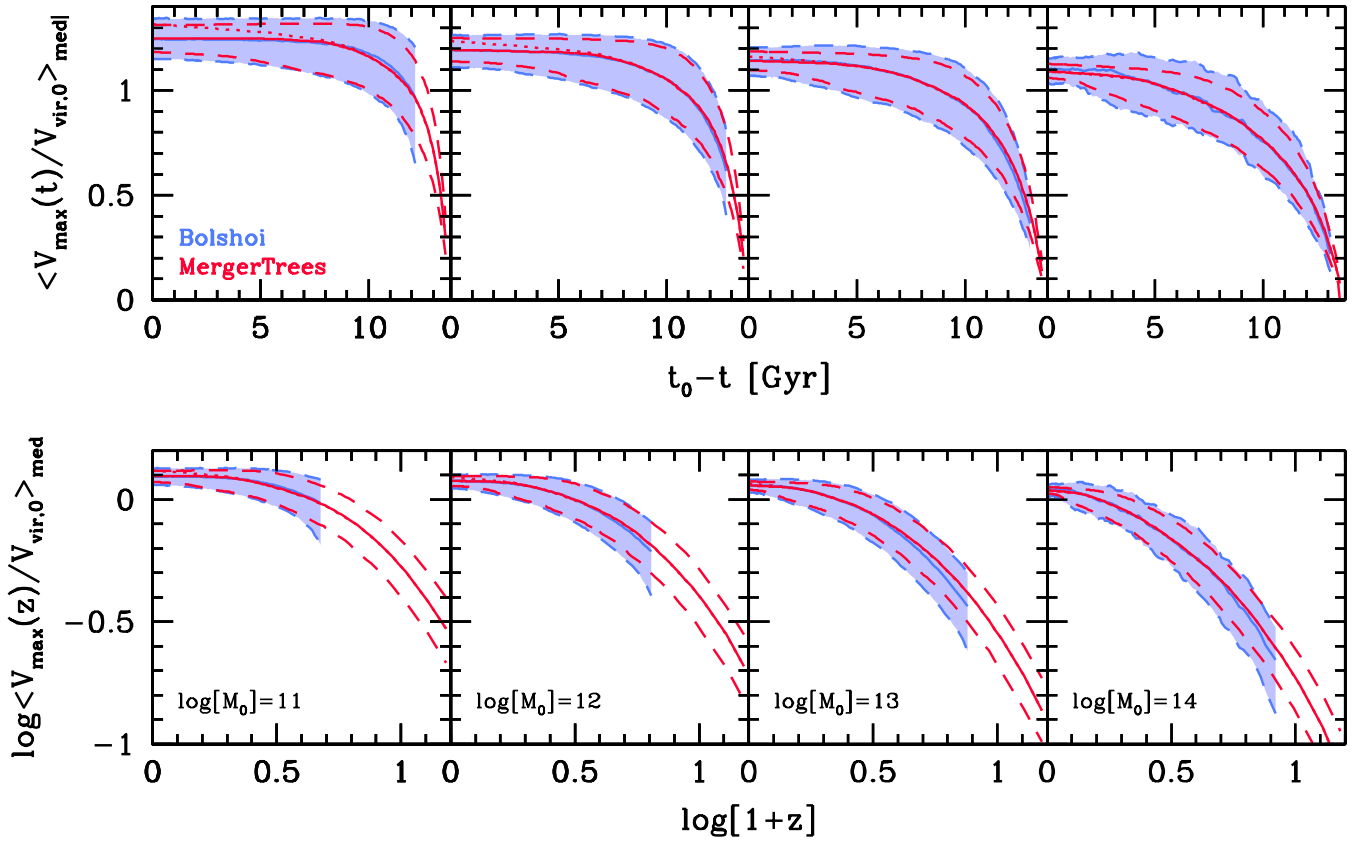
Figure 9. Same as Fig. 3, but for the median PWGHs, $V_{\mathrm{max}}(t)/V_{\mathrm{vir},0}$. The dotted, red lines show the median PWGHs obtained from MergerTrees with the original concentration-mass-redshift relation of Zhao et al. (2009; Eq. [11]), which somewhat overshoots V_{max} of low mass haloes at late times, simply because it overpredicts their concentrations (see §3.3).

et al. (2009) and Giocoli et al. (2012) are inadequate to describe our MAHs because they used a different definition for the main progenitor. We therefore start by developing a new, universal model, which then serves as the basis for computing the PWGHs using Eq. (16) above. Our model is motivated by the fact that simulations and EPS studies have shown that the unevolved subhalo mass function is (almost) universal (Lacey & Cole 1993; Zentner & Bullock 2003; van den Bosch et al. 2005; Giocoli, Tormen & van den Bosch 2008; Li & Mo 2009; Yang et al. 2011). This means that, statistically speaking, all haloes grow in mass by accreting the same haloes when expressed in terms of their normalized mass M_{p}/M_0 (here M_{p} is the progenitor mass, and M_0 is the final host mass). Hence, average MAHs for haloes of different M_0 and/or different cosmology only differ from each other because they accrete those progenitors at different times (see also Neistein & Dekel 2008a; Genel et al. 2009; Neistein et al. 2010; Yang et al. 2011). This suggests that one should be able to transform the average or median MAH for a halo of mass, $M_{0,\mathrm{r}}$, and cosmology, $\mathcal{C}_{\mathrm{r}}$, to that of a halo of another mass and cosmology, $(M_{0,\mathrm{t}}, \mathcal{C}_{\mathrm{t}})$, via a simple transformation of the time-coordinate (cf., Neistein et al. 2010). Here the subscripts 'r' and 't' refer to the 'reference' and 'target' MAH, respectively. Using ψ as shorthand for either the median or the average MAH, i.e., $\psi(z) \equiv \langle M(z)/M_0 \rangle_{\mathrm{med}}$ or $\psi(z) \equiv \langle M(z)/M_0 \rangle$, respectively, one can then write that

$$\psi(z|M_{0,\mathrm{t}}, z_{0,\mathrm{t}}, \mathcal{C}_{\mathrm{t}}) = \psi(z'|M_{0,\mathrm{r}}, z_{0,\mathrm{r}}, \mathcal{C}_{\mathrm{r}}), \qquad (17)$$

and all that remains is to find the appropriate time-transformation, $z = z(z')$, and to identify a reference MAH.

4.1 Self-similarity in time

In the EPS formalism, there is a natural variable for which the (conditional) mass function of dark matter haloes is invariant with halo mass and cosmology. This variable is $\delta_{\mathrm{c}}(z)/\sigma(M)$, where $\delta_{\mathrm{c}}(z) = 1.686/D(z)$ and $\sigma^2(M)$ is the mass variance. This suggests that a natural choice for the time transformation $z' \to z(z')$ is given by $\omega_{\mathrm{t}}(z) = \omega_{\mathrm{r}}(z')$, where

$$\omega(z) = \omega(z|M, M_0, z_0) \equiv \frac{\delta_{\mathrm{c}}(z) - \delta_{\mathrm{c}}(z_0)}{\sqrt{\sigma^2(M) - \sigma^2(M_0)}}. \qquad (18)$$

Indeed, as shown by Lacey & Cole (1993), the distribution of halo formation times takes on a form that is (almost) independent of halo mass and/or cosmology[§§] when expressed in terms of ω. Although we find that this scaling (also promoted by Neistein et al. 2010) captures much of the trends that MAHs display with mass and cosmology, it lacks sufficient precision and becomes progressively worse for larger mass and/or cosmology differences between reference and target, especially at larger redshifts. This should not come

---

[§§] ω only has a weak dependence on the slope of the matter power spectrum.
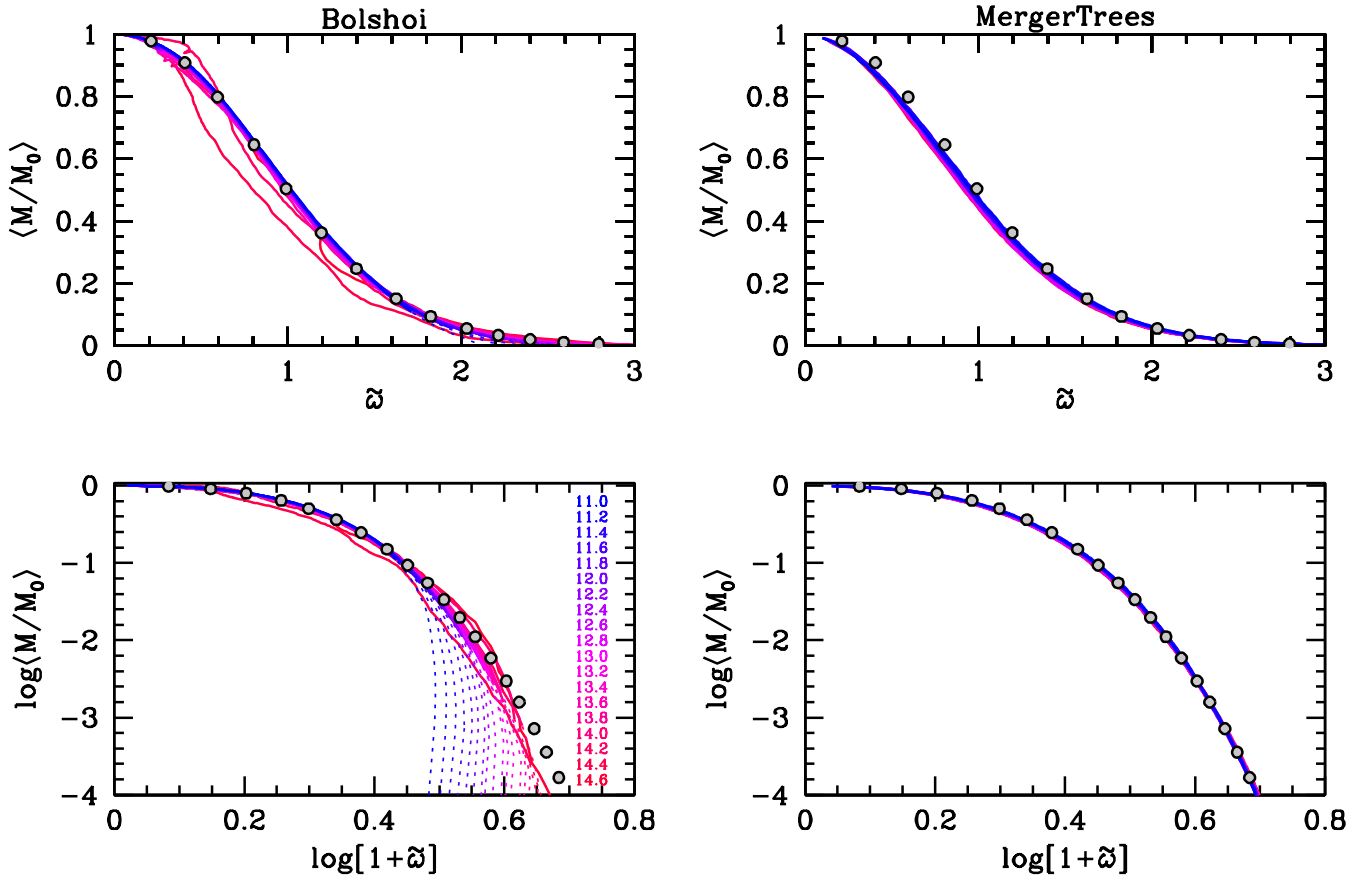
Figure 10. Same as Fig. 2, but this time the average MAHs are plotted as function of the time variable $\widetilde{\omega}$, defined by Eq. (19). Note how all MAHs collapse on top of each other, indicating that the average (and median) MAHs of dark matter haloes have a universal shape. The few curves in the left-hand panel that do not fall on top of the others correspond to massive haloes, for which the averages are noisy due to small number statistics. The gray circles indicate the universal relation between $\widetilde{\omega}$ and $\psi = \langle M/M_0 \rangle$, which is well fitted by Eq. (20) and with the best-fit parameters listed in Table 1.

entirely as a surprise. After all, it is well-known that EPS predicts halo assembly to occur later than what is found in numerical simulations (e.g. van den Bosch 2002a; Lin, Jing & Lin 2003; Neistein et al. 2006). Related to this is the fact that EPS, when based on spherical collapse, yields (conditional) halo mass functions that fail to accurately match simulation data. In fact, this is the reason why the Parkinson et al. (2008) algorithm that we use to construct our merger trees relies on a progenitor mass function that multiplies the EPS prediction with the perturbing function $G(M, M_0, z_0)$ given by Eq. (10).

Hence, a logical next step is to consider a time-transformation $\widetilde{\omega}_t(z) = \widetilde{\omega}_r(z')$, where

$$\widetilde{\omega}(z|M, M_0, z_0) \equiv \omega(z|M, M_0, z_0)\, G^{\gamma}(M, M_0, z_0) \qquad (19)$$

with γ a free parameter. Indeed, after some trial and error we find that using $\gamma = 0.4$ results in extremely accurate transformations from one MAH to another. In particular, this transformation not only works for the Bolshoi simulation, but also can be used to transform MAHs from one ΛCDM cosmology to the other. It implies that the average and/or median MAH has a universal form when written as $\psi(\widetilde{\omega})$. Since $\widetilde{\omega}$ itself depends on ψ (i.e., $M = \psi M_0$), this universal form is a parametric equation that has to be solved numerically (see Appendix C for details).

Fig. 10 shows the same average MAHs as in Fig. 2, but this time plotted as function of $\widetilde{\omega}$. Left and right-hand panels plot MAHs obtained from Bolshoi and MergerTrees, respectively. As in Fig. 2, dotted curves are the extensions of the Bolshoi MAHs to the redshift range where fewer than 90% of the individual MAHs can be traced, and are therefore heavily influenced by resolution effects. Note how all MAHs fall on top of each other, reflecting the universal character of $\psi(\widetilde{\omega})$.

In order to characterize the universal, parametric form of $\psi(\widetilde{\omega})$ we fit the inverse relation, $\widetilde{\omega}(\psi)$, using the following functional form

$$\mathcal{F}(\psi) \equiv a_1 \left[1 - a_2 \log \psi\right]^{a_3} \left(1 - \psi^{a_4}\right)^{a_5} \qquad (20)$$

where $(a_1, a_2, ..., a_5)$ are treated as free parameters. Since the Bolshoi results are arguably more reliable than MergerTrees, we fit the free parameters using Bolshoi data, but only at $z \leq 2$ ($\widetilde{\omega} \lesssim 1.5$). At higher redshifts, the Bolshoi data either suffers from limited mass resolution (in the case of low mass haloes), or from a small sample size (in the case of massive haloes). Therefore, we complement the simulation data with MergerTrees results for $z > 2$. The resulting best-fit parameters are given in Table 1, both for the average and the median MAHs. The corresponding best-fit relation
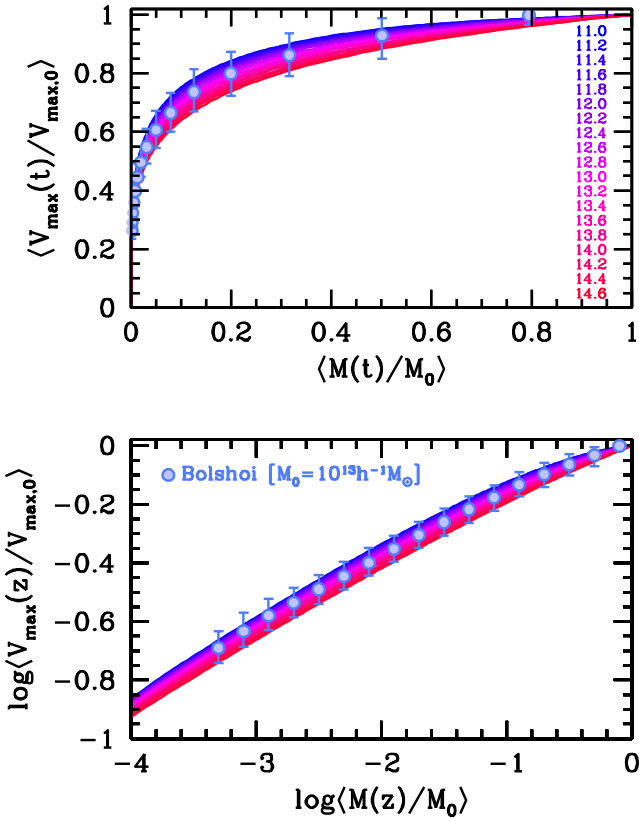
Figure 8. The average $V_{\mathrm{max}}(t)/V_{\mathrm{max},0}$ as function of the average $M(t)/M_0$. Lines of different color, which can barely be discerned from one another, correspond to the results obtained using MergerTrees for haloes of different mass, M_0; color coding is the same as in Figs. 2 and 7, and is indicated in the top panel. Solid circles are results obtained from the Bolshoi simulation for haloes with $\log[M_0/(h^{-1}\mathrm{M}_\odot)] \in [12.9, 13.1]$; only plotting results for the range where $> 90\%$ of the MAHs are resolved. Errorbars mark the 68 percent interval from the distribution of *individual* MAHs in this mass range. These results clearly illustrate the inside-out assembly of dark matter haloes, with the central potential well forming well before most of the mass is in place.

Table 1. Parameters of Universal MAHs

MAH	a_1	a_2	a_3	a_4	a_5
average	3.295	0.198	0.754	0.090	0.442
median	1.928	0.424	0.768	0.148	0.310

Best-fit parameters for Eq. (20) describing the average (upper row) and median (lower low) MAHs.

for the average MAH is shown as solid dots in Fig. 10, which accurately fit the Bolshoi and MergerTrees results.

As detailed in Appendix C, by numerically solving

$$\mathcal{F}(\psi) = \widetilde{\omega}(\psi, z), \qquad (21)$$

either for ψ at given z, or for z at given ψ, one can compute the average or median MAHs for a host halo of any mass, M_0, at any redshift, z_0, and for any (ΛCDM) cosmology. Using Eq. (16), these can subsequently be used to compute the corresponding average or median PWGH.

Fig. 11 plots the median PWGHs for haloes of four different host halo masses in the Bolshoi cosmology. Solid circles are the results obtained from the Bolshoi simulation (using a halo mass bin width of 0.2dex), while crosses are the results obtained using MergerTrees. The solid, colored curves are the predictions for these median PWGHs obtained using our universal model described above. As is evident, the model is in excellent agreement with the results from MergerTrees, which in turn are in excellent agreement with the simulation results. We have used MergerTrees to test the universal model for halo masses and flat ΛCDM cosmologies spanning the ranges $10^9 \ h^{-1}\mathrm{M}_\odot \lesssim \mathrm{M}_0 \lesssim 10^{15} \ h^{-1}\mathrm{M}_\odot$, $0.1 \leq \Omega_{\mathrm{m},0} \leq 0.5$, $0.6 \leq \sigma_8 \leq 1.0$, $0.9 \leq n_{\mathrm{s}} \leq 1.0$, and $0.6 \leq h \leq 0.8$. This amply covers the range of cosmologies in agreement with current observations. For each of those cases we find similar levels of agreement as shown in Fig. 11. In general, the model agrees with the predictions from MergerTrees to better than a few percent.

Appendix C gives a detailed step-by-step description of how to compute the average and/or median MAHs and PWGH using this universal model. In addition, it also describes how this model can be used to compute halo formation redshifts, z_{f}, for any value of f.

4.2 Mass Accretion Rates

The universal model for the MAHs presented above can also be used to analytically compute the median or average mass accretion rates for haloes of any mass, at any redshift, and for any ΛCDM cosmology. Differentiating (21) with respect to ψ yields that

$$\frac{\mathrm{d}\psi}{\mathrm{d}t} = \frac{\partial \widetilde{\omega}}{\partial t} \left[\frac{\mathrm{d}\mathcal{F}}{\mathrm{d}\psi} - \frac{\partial \widetilde{\omega}}{\partial \psi} \right]^{-1}, \qquad (22)$$

which, after some algebra, can be written in the form

$$\langle \dot{M} \rangle = \frac{M}{t} \frac{\mathcal{D}}{\mathcal{H} + \mathcal{S}}, \qquad (23)$$

Here the angle brackets refer to either the median or the average, depending on whether ψ represents the median or the average, the dot indicates the time derivative, and $\mathcal{D}$, $\mathcal{H}$, and $\mathcal{S}$ are given by

$$\mathcal{D} = \frac{\partial \ln D}{\partial \ln t} \left[\frac{\delta_{\mathrm{c}}(t)}{\delta_{\mathrm{c}}(t) - \delta_{\mathrm{c}}(t_0)} - 0.004 \right], \qquad (24)$$

$$\mathcal{S} = \left| \frac{\partial \ln \sigma}{\partial \ln M} \right| \left[\frac{\sigma^2(\psi M_0)}{\sigma^2(\psi M_0) - \sigma^2(M_0)} - 0.152 \right], \qquad (25)$$

and

$$\mathcal{H} = -\frac{\mathrm{d} \ln \mathcal{F}}{\mathrm{d} \ln \psi} = 0.4343 \frac{a_2 a_3}{1 - a_2 \log \psi} + \frac{a_4 a_5 \psi^{a_4}}{1 - \psi^{a_4}} \qquad (26)$$

Hence, $\mathcal{D}$ describes the dependence on the linear growth rate, $D(t)$, $\mathcal{S}$ the dependence on the mass variance, $\sigma^2(M)$, and $\mathcal{H}$ is related to the functional form of the universal MAH.

Fig. 12 plots the average accretion rates for the main progenitors of host haloes of different present day mass, M_0. Solid circles are the results obtained from the Bolshoi simulation, by numerically differentiating the corresponding, average MAHs. The colored, solid curves are the model predictions computed using Eq. (23). Results are shown both as
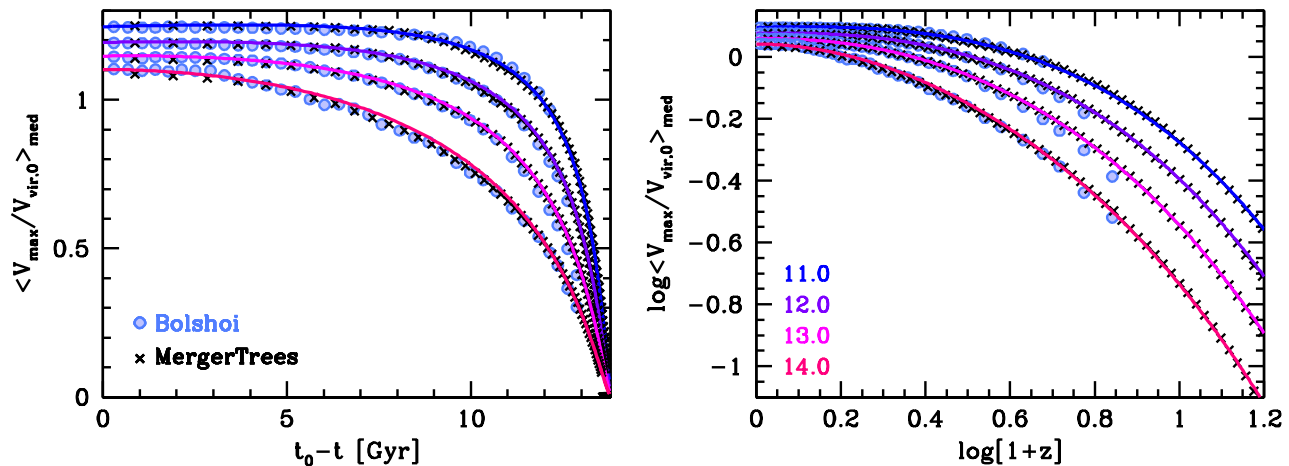
Figure 11. Median PWGHs, $\langle V_{\max}/V_{\mathrm{vir},0}\rangle$ as function of lookback time (left-hand panel) and redshift (right-hand panel). Blue dots and black crosses are the results obtained from the Bolshoi simulation and MergerTrees, respectively, while the solid, colored lines are the predictions from our universal model described in §4.1 and Appendix C. Results are shown for four different host halo masses, as indicated in the right-hand panel. Note the exquisite mutual agreement.

function of lookback time (left-hand panel) and as function of $\log[1+z]$ (right-hand panel), to better accentuate the behavior at late and early times, respectively. As is evident, the model predictions are in excellent agreement with the simulation results, providing further support for our universal model.

The dashed curves are the model predictions of Fakhouri et al. (2010), which are given by

$$\langle \dot{M}\rangle = 47.6\,h^{-1}\,\mathrm{M_\odot yr^{-1}} \left(\frac{M}{10^{12}h^{-1}\,\mathrm{M_\odot}}\right)^{1.1} (1+1.11z)$$
$$\times \sqrt{\Omega_{\mathrm{m},0}(1+z)^3 + \Omega_{\Lambda,0}}\,. \tag{27}$$

These slightly underpredict the mass accretion rates at high z and overpredict $\langle \dot{M}\rangle$ at late times. We emphasize, though, that although Fakhouri et al. have explicitly written how their average mass accretion rate depends on $\Omega_{\mathrm{m},0}$ and $\Omega_{\Lambda,0}$, their results are strictly *only* valid for the cosmology adopted for the Millennium simulation, which differs somewhat from the Bolshoi cosmology. Indeed, using our model to compute $\langle \dot{M}\rangle$ for the Millennium cosmology, we obtain results that are in much better agreement with Eq. (27), but only at large redshifts; the discrepancy at late times ($t_0 - t \lesssim 3\mathrm{Gyr}$) remains virtually unaltered. Hence, we conclude that the latter most likely reflects a discrepancy that arises from the use of different halo finders and different algorithms to construct halo merger trees (see discussion in §2.4).

5 CONCLUSIONS

We have presented a detailed study of how dark matter haloes assemble their mass and grow their (central) potential well. For an NFW profile, the latter is directly proportional to the square of the maximum circular velocity, which is why we characterize halo growth via the mass accretion histories (MAHs), $\langle M/M_0\rangle$, and the potential well growth histories (PWGHs), $\langle V_{\max}/V_{\mathrm{vir},0}\rangle$. Surprisingly the latter have received little attention in the literature to this date, despite the fact that $V_{\max}$ has the advantange that it can be more

reliably and robustly measured than halo mass (both in simulations and in real data), and is defined without ambiguity, freeing it from issues such as 'pseudo-evolution' that hamper interpretations of the MAHs. In addition, $V_{\max}$ is often used as the halo parameter of choice in abundance matching, suggesting that it may be a better 'regulator' of galaxy formation than halo mass.

We have used results from both the large Bolshoi simulation, as well as from merger trees constructed using the Parkinson et al. (2008) algorithm. We have supplemented the latter with a method, developed by Jiang & van den Bosch (2014b), to compute the maximum circular velocity, $V_{\max}$, of the main progenitor as function of time. This method uses the universal model between halo concentration and halo formation time developed by Zhao et al. (2009). We have demonstrated that both methods yield results that are overall in excellent agreement, both in terms of the average or median as well as in terms of the scatter. However, we also identified a few small inconsistencies. First of all, MergerTrees somewhat underpredict the halo-to-halo variance at late times (Fig. 3). Most likely this is a manifestation of the fact that host haloes in simulations can loose mass due to 'ejected subhaloes', something that is not accounted for in MergerTrees. Since most of this 'lost mass' remains bound to the host halo (and will re-accrete at some later time), we do not consider this a particular failure of MergerTrees, but rather a complication associated with how to assign mass to dark matter haloes. Secondly, in order to match the slope of the concentration-mass relation, we had to slightly modify the concentration-formation time relation of Zhao et al. (2009). This is most likely a consequence of the fact that Zhao et al. used a different definition for main progenitor than adopted here. Hence, our concentration-formation time relation presented here (Eq. [14]) may be considered a recalibration of the Zhao et al. model for cases in which the main progenitor is defined as the most-massive, rather than the most-contributing, progenitor. Finally, the Bolshoi simulation reveals distributions of halo concentration at fixed halo mass that deviate from log-normal, in that they have an extended tail towards low-concentration haloes. Such a tail
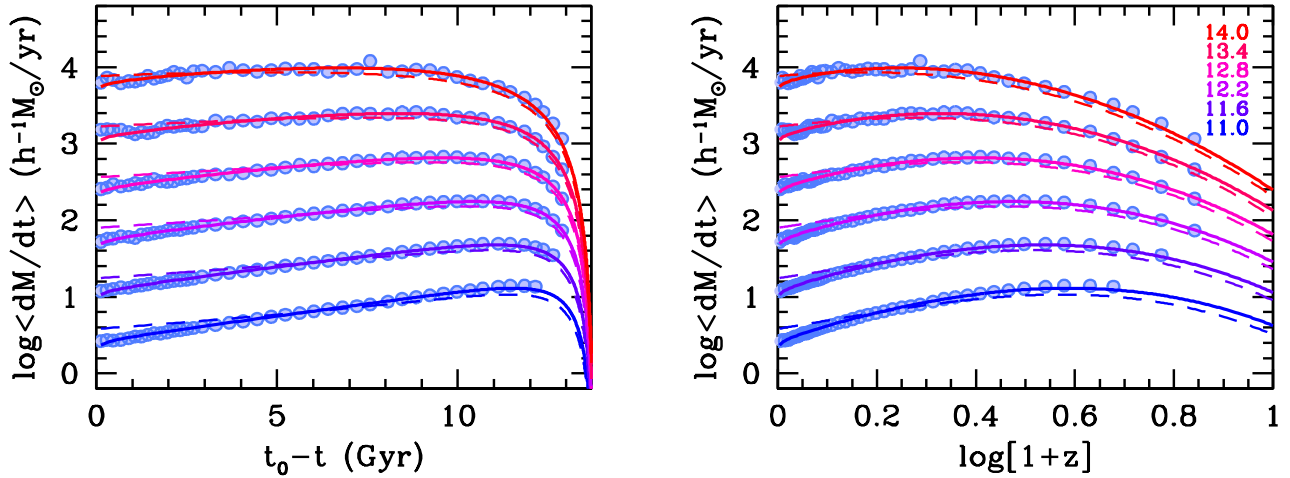
Figure 12. Average halo accretion rates, $\langle \mathrm{d}M/\mathrm{d}t \rangle$, for the main progenitors of host haloes of different present day mass, M_0, as indicated. Results are shown both as function of lookback time (left-hand panel) and as function of $\log[1+z]$ (right-hand panel), to better accentuate the behavior at late and early times, respectively. Solid circles are the results obtained from the Bolshoi simulation, by numerically differentiating the corresponding, average MAHs. The colored, solid curves are the predictions from our universal model (Eq. [23]). The colored, dashed curves are the corresponding model predictions of Fakhouri et al. (2010), given by Eq. (27), and are shown for comparison.

is absent in the distributions predicted using MergerTrees, and is due to unrelaxed haloes. As a consequence, MergerTrees slightly underpredicts the halo-to-halo variance in the PWGHs, but the effect is small.

In agreement with numerous previous studies, we find that more massive haloes assemble later. This not only holds for how they assemble their mass, but also for how they build their central potential well. We show that the latter precedes the former, illustrating the inside-out build-up of dark matter haloes. We show that the haloes follow a tight relation between $M(t)/M_0$ and $V_{\mathrm{max}}(t)/V_{\mathrm{max},0}$, which is basically a manifestation of the fact that dark matter haloes follow a universal density profile. As a rule of thumb, *the maximum circular velocity of a halo's main progenitor is already half the present day value by the time it has accreted only about 2 percent of its final mass.* Consequently, dark matter haloes rapidly grow their central potential, at early times, followed by an extensive period in which the central potential deepens only very slowly. During this 'quiescent era' the halo mainly grows its outskirts (see also Li et al. 2007).

In addition to a comparison with the results from the Bolshoi simulation, we have also compared the predictions of MergerTrees with the universal models for the median MAHs of Zhao et al. (2009) and Giocoli et al. (2012). We find that all models perfectly agree with each other, and with the Bolshoi simulation results, at low redshift ($z \lesssim 1.5$). At higher z, the models of Zhao et al. (2009) and Giocoli et al. (2012) slightly underpredict the median MAHs compared to Bolshoi and to MergerTrees. Motivated by these findings we have developed a new, universal model for both the average and median MAH, which can also be used to predict the corresponding PWGH. The model is motivated by the fact that simulations and EPS-based merger trees have shown that the unevolved subhalo mass function (i.e., the mass function of haloes accreted directly by the main progenitor) is universal. This means that, statistically speaking, all haloes grow in mass by accreting the same haloes when normalized in mass by that of the final host halo. Hence,

the average (and median) MAHs for haloes of different mass and/or different cosmology only differ from each other because they accrete those progenitors at different times. This suggests that MAHs should have a universal form when expressed in terms of a 'universal time'. We have found this universal time to be given by

$$\widetilde{\omega}(z|M, M_0, z_0) = \frac{\delta_{\mathrm{c}}(z) - \delta_{\mathrm{c}}(z_0)}{\sqrt{\sigma^2(M) - \sigma^2(M_0)}} G^{0.4}(M, M_0, z_0) \quad (28)$$

with $G(M, M_0, z_0)$ the perturbing function used in the Parkinson et al. (2008) method to define the progenitor mass function. We have shown that, when plotted as function of $\widetilde{\omega}$, the average and median MAHs have a universal (parametric) form given by $\mathcal{F}(\psi) = \widetilde{\omega}(\psi, z)$. Here ψ is shorthand for either the average or the median MAH, and $\mathcal{F}(\psi)$ is a universal function that is accurately fit by Eq. (20) with the best-fit parameters listed in Table 1. As described in Appendix C, this universal model for the MAH can also be used to compute the average or median PWGH. We have tested this new, easy-to-use, universal model, against the Bolshoi simulation results and against the predictions based on MergerTrees, and found it to predict MAHs and PWGHs with percent level accuracy over the entire range of halo masses and ΛCDM cosmologies tested (see §4.1 for details).

The fact that the unevolved subhalo mass function is universal not only implies an universal MAH, it also implies that *the entire halo merger tree is invariant*; when expressing all progenitor masses in units of the final host halo mass, and all times in term of $\widetilde{\omega}$, one obtains a universal merger tree that can be used to represent the merger tree for a halo of any mass in any (ΛCDM) cosmology. This has important applications. For instance, semi-analytical models for galaxy formation no longer have to use large samples of merger trees to properly sample the entire population of host haloes; rather, they can read in a sample of ∼ 100 merger trees for a halo of one particular mass (to sample the halo-to-halo variance), and rescale these to represent the merger trees

for any other halo mass. In addition, changing cosmological parameters no longer requires running a new set of merger trees, as the existing set is trivially rescaled.

Finally, differentiating the universal MAH, we obtain a universal, fully analytical model for the average (or median) mass accretion rate of dark matter haloes, which is in excellent agreement with results from the Bolshoi simulation. Unlike the fitting formula presented in Neistein & Dekel (2008a,b), Dekel et al. (2009), Genel et al. (2009), McBride et al. (2009) and Fakhouri et al. (2010), all of which are only valid for the particular cosmology adopted in the Millennium simulation, this universal accretion rate is valid for any ΛCDM cosmology.

We conclude by emphasizing that our results demonstrate the utility of semi-analytical modeling in an era of research that increasingly relies upon numerical results taken directly from simulations. Semi-analytical models, such as that presented here, allow us to probe a large dynamic range in mass and to explore cosmological dependencies that would otherwise be excessively expensive in terms of CPU requirements. In addition, semi-analytical models, by resorting to simplified prescriptions of the underlying dynamics, are extremely useful in gaining insight and understanding. The universal model developed here is a clear example of the power of such an approach.

ACKNOWLEDGMENTS

REFERENCES

Avila-Reese V., Firmani C., Hernández X., 1998, ApJ, 505, 37
Baugh C.M., Cole S., Frenk C.S., 1996, MNRAS, 283, 1361
Behroozi P.S., Wechsler R.H., Wu H.-Y., 2013a, ApJ, 762, 31
Behroozi P. S., Wechsler R. H., Wu H.-Y., Busha M.T., Klypin A.A., Primack J.R., 2013b, ApJ, 763, 18
Behroozi P.S., Wechsler R.H., Conroy C., 2013c, ApJ, 770, 57
Behroozi P.S., Silk J., preprint (arXiv:1404.5299)
Bond J. R., Cole S., Efstathiou G., Kaiser N., 1991, ApJ, 379, 440
Boylan-Kolchin M., Springel V., White S.D.M., Jenkins A., 2010, MNRAS, 406, 896
Bryan G., Norman M., 1998, ApJ, 495, 80
Cohn J.D., White M., 2005, Astroparticle Phys. 24, 316
Cole S., Lacey C. G., Baugh C. M., Frenk C. S., 2000, MNRAS, 319, 168
Cole S., Helly J., Frenk C. S., Parkinson H., 2008, MNRAS, 383, 546
Cuesta A.J., Prada F., Klypin A., Moles M., 2008, MNRAS, 389, 385
Diemand J., Kuhlen M., Madau P., 2007, ApJ, 667, 859
Diemer B., More S., Kravtsov A.V., 2013, ApJ, 766, 25
Diemer B., Kravtsov A.V., 2014, preprint (arXiv:1401.1216)

Dutton A., van den Bosch F.C., Dekel A., Courteau S., 2007, ApJ, 654, 27
Eisenstein D.J., Loeb A., 1996, ApJ, 459, 432
Fakhouri, O., Ma, C.-P., 2008, MNRAS, 386, 577
Fakhouri, O., Ma, C.-P., Boylan-Kolchin M., 2010, MNRAS, 406, 2267
Firmani C., Avila-Reese V., 2000, MNRAS, 315, 457
Gao L., White S.D.M., Jenkins A., Stoehr F., Springel V., 2004, MNRAS, 355, 819
Gao L., Springel V., White S.D.M., 2005, MNRAS, 363, 66
Geha M., Blanton M.R., Yan R., Tinker J.L., 2012, ApJ, 757, 85
Genel S. et al., 2008, ApJ, 688, 789
Genel S., Genzel R., Bouché N., Naab T., Sternberg A., 2009, ApJ, 701, 2002
Giocoli C., Moreno J., Sheth R.K., Tormen G., 2007, MNRAS, 376, 977
Giocoli C., Tormen G., van den Bosch F.C., 2008, MNRAS, 386, 2135
Giocoli C., Tormen G., Sheth R.K., van den Bosch F.C., 2010, MNRAS, 404, 502
Giocoli C., Tormen G., Sheth R. K., 2012, MNRAS, 422, 185 (G12)
Giocoli C., Marulli F., Baldi M., Moscardini L., Metcalf R.B., 2013, MNRAS, 434, 2982
Harker G., Cole S., Helly J., Frenk C.S., Jenkins A., 2006, MNRAS, 367, 1039
Hearin A.P., Zentner A.R., Berlind A.A., Newman J.A., 2013, MNRAS, 433, 659
Hearin A.P., Watson D.F., 2013, MNRAS, 435, 1313
Hearin A.P., Watson D.F., van den Bosch F.C., 2014, preprint (arXiv:1404.6524)
Helly J.C., Cole S., Frenk C.S., Baugh C.M., Benson A., Lacey C., 2003, MNRAS, 338, 903
Jiang F., van den Bosch F.C., 2014a, MNRAS, 440, 193
Jiang F., van den Bosch F.C., 2014b, MNRAS, (arXiv:1403.6827)
Kauffmann G., White S.D.M., Guiderdoni B., 1993, MNRAS, 264, 201
Klypin A., Holtzman J., 1997, preprint (arXiv:astro-ph/9712217)
Klypin A.A., Trujillo-Gomez S., Primack J.R., 2011, ApJ, 740, 102
Knebe A., Knollmann S.R., Muldrew S.I., Pearce F.R., Aragon-Calvo M.A., Ascasibar Y., Behroozi P.S., Ceverino D., 2011, MNRAS, 415, 2293
Knebe A., Pearce F. R., Lux H., Ascasibar Y., Behroozi P. S., Casado J., Moran C. C., Diemand J., 2013, MNRAS, 435, 1618
Kravtsov A.V., Klypin A.A., Khokhlov A.M., 1997, ApJS, 111, 73
Lacey C.G., Cole S., 1993, MNRAS, 262, 627
Li Y., Mo H.J., van den Bosch F.C., Lin W.P., 2007, MNRAS, 379, 689
Li Y., Mo H.J., Gao L., 2008, MNRAS, 389, 1419
Li Y., Mo H.J., 2009, preprint (arXiv:0908.0301)
Lin W. P., Jing Y. P., Lin L., 2003, MNRAS, 344, 1327
Ludlow A.D., et al., 2013, MNRAS, 432, 1103
Macciò A.V., Dutton A.A., van den Bosch F.C., Moore B., Potter D., Stadel J., 2007, 2007, MNRAS, 378, 55
Maccio A.V., Dutton A.A., van den Bosch F.C., 2008, MNRAS, 391, 1940
Maulbetsch C., Avila-Reese V., Colín P., Gottlöber S., Khalatyan A., Steinmetz M., 2007, ApJ, 654, 53
McBride J., Fakhouri O., Ma C.-P., 2009, MNRAS, 398, 1858
Mo H., van den Bosch F.C., White S.D.M., 2010, Galaxy Formation and Evolution, Cambridge University Press
Navarro J.F., Frenk C.S., White S.D.M., 1997, ApJ, 490, 493
Neistein E., van den Bosch F.C., Dekel A., 2006, MNRAS, 372, 933
Neistein E., Dekel A., 2008a, MNRAS, 383, 615

Neistein E., Dekel A., 2008b, MNRAS, 388, 1792

Neistein E., Maccío A.V., Dekel A., 2010, MNRAS, 403, 2717

Neto A. F., Gao L., Bett P., Cole S., Navarro J. F., Frenk C. S., White S. D. M., Springel V., et al. , 2007, MNRAS, 381, 1450

Nusser A., Sheth R.K., 1999, MNRAS, 303, 685

Parkinson H., Cole S., Helly J., 2008, MNRAS, 383, 557 (P08)

Reddick R.M., Wechsler R.H., Tinker J.L., Behroozi P.S., 2012, ApJ, 771, 30

Sheth R.K., Tormen G., 2004, 1999, MNRAS, 350, 1385

Somerville R.S., Kolatt T.S., 1999, MNRAS, 305, 1

Springel V., et al., 2005, Nature, 435, 629

Srisawat C. et al., 2013, MNRAS, 436, 150

Tasitsiomi A., Kravtsov A.V., Gottlöber S., Klypin A.A., 2004, ApJ, 607 125

Trujillo-Gomez S., Klypin A., Primack J., Romanowsky A.R., 2011, ApJ, 742, 16

van den Bosch F.C., 2000, ApJ, 530, 177

van den Bosch F.C., 2001, MNRAS, 327, 1334

van den Bosch F.C., 2002a, MNRAS, 331, 98 (vdB02)

van den Bosch F.C., 2002b, MNRAS, 332, 456

van den Bosch F.C., Tormen G., Giocoli C., 2005, MNRAS, 359, 1029

van den Bosch, F. C., Jiang F., 2014, preprint (arXiv:1403.6835)

Wang H., Mo H.J., Jing Y.P., 2009a, MNRAS, 396, 2249

Wang Y., Yang X., Mo H.J., van den Bosch F.C., Katz N., Pasquali A., McIntosh D.H., Weinmann S.M., 2009b, ApJ, 697, 247

Watson D.F., Hearin A.P., Berlind A.A., Becker M.R., Behroozi P.S., Skibba R.A., Reyes R., Zentner A.R., 2014, preprint (arXiv:1403.1578)

Wechsler R.H., Bullock J.S., Primack J.R., Kravtsov A.V., Dekel A., 2002, ApJ, 568, 52

Wetzel A.R., Tinker J.L., Conroy C., van den Bosch, F.C., 2014, MNRAS, 439, 2687

Wu H.-Y., Hahn O., Wechsler R.H., Behroozi P.S., Mao Y.-Y., 2013, ApJ, 767, 23

Yang X., Mo H.J., Zhang Y., van den Bosch F.C., 2011, ApJ, 741, 13

Zemp M., 2013, preprint (arXiv:1312.4629)

Zentner A.R., Bullock J.S., 2003, ApJ, 598, 49

Zentner A.R., Hearin A.P., van den Bosch F.C., 2013, MNRAS, submitted (arXiv:1311.1818)

Zhang J., Ma C.-P., Fakhouri O., 2008, MNRAS, 387, L13

Zhao D.H., Jing Y.P., Mo H.J., Börner G., 2003a, ApJ, 597, 9

Zhao D.H., Mo H.J., Jing Y.P., Börner G., 2003b, MNRAS, 339, 12

Zhao D.H., Jing Y.P., Mo H.J., Börner G., 2009, ApJ, 707 354 (Z09)

APPENDIX A: EJECTED HALOES

Fig. A1 compares the average MAHs obtained from the Bolshoi simulation for host haloes (left-hand panels), subhaloes (middle panels), and ejected haloes (right-hand panels). Once again different colors correspond to different bins of $z = 0$ halo mass (each bin is 0.2dex wide), as indicated. We only plot results for mass bins for which we have at least 20 haloes per category, which restricts the comparison to haloes with $M_0 \leq 10^{13.7}\ h^{-1}\mathrm{M}_\odot$.

We emphasize that it is not necessarily particularly meaningful to average the MAH for subhaloes or ejected haloes in bins of present-day mass; however, the main point of Fig. A1 is to demonstrate that subhaloes and ejected haloes have MAHs that differ substantially from those of host haloes of the same present-day mass and therefore have

to be excluded from the samples of 'host haloes'. Although this is pretty obvious for subhaloes, it is less clear for ejected host haloes, and virtual all studies to date of the MAHs of dark matter haloes based on numerical simulations have included ejected haloes in their samples. Although their fractional contribution is small (see Fig. 1), their average MAHs are sufficiently different that they can still cause a mild (but significant) distortion of the averages, especially for low mass haloes. Motivated largely by the work of Wang et al. (2009b), Geha et al. (2012), Wetzel et al. (2014), and others, we believe that ejected haloes are more akin to subhaloes than to host haloes, and we therefore remove them from our sample of host haloes.

APPENDIX B: COSMOLOGY DEPENDENCE

As discussed in §3.2, various studies have presented fitting functions for the average and/or median MAHs (or their time-derivatives) based on one particular numerical simulation (e.g., Neistein & Dekel 2008a; McBride, Fakhouri & Ma 2009; Genel et al. 2009; Fakhouri et al. 2010; Wu et al. 2013). In this Appendix, we demonstrate that the average MAHs depend appreciably on cosmology, and that these fitting functions are therefore only applicable for the cosmology used to run the numerical simulation.

Fig. B1 plots the average MAHs for a halo of mass $M_0 = 10^{13} h^{-1}\mathrm{M}_\odot$ in different, flat ΛCDM cosmologies. Each average MAH is obtained averaging over 2000 realizations of MergerTrees. Upper and lower panels plot $\langle M(t)/M_0 \rangle$ as function of lookback time and $\log\langle M(z)/M_0 \rangle$ as function of $\log[1+z]$, accentuating the behaviors at late and early times, respectively. The base-cosmology has $\Omega_{\mathrm{m},0} = 1 - \Omega_{\Lambda,0} = 0.3$, $\Omega_{\mathrm{b},0} = 0.045$, $h = 0.7$, $\sigma_8 = 0.8$ and $n_\mathrm{s} = 1.0$, and is represented by the magenta curves. The other curves are the average MAHs, for haloes of the same present-day mass, in cosmologies in which only one parameter is changed with respet to this base cosmology: in the left-hand panel we change $\Omega_{\mathrm{m},0}$ from 0.1 to 0.6 (note that we change $\Omega_{\Lambda,0}$ as well, to assure a flat geometry), in the middle panel we change σ_8 from 0.6 to 1.0, and in the right-hand panel we change the spectral index, n_s, from 0.8 to 1.2.

Changing the cosmological matter density, $\Omega_{\mathrm{m},0}$, changes the linear growth rate. As a result, haloes in low-$\Omega_{\mathrm{m},0}$ cosmologies assemble earlier than in a high-$\Omega_{\mathrm{m},0}$ cosmology, when expressed in terms of lookback time. Note, though, that this trend is reversed when plotted as function of redshift, due to the fact that changes in $\Omega_{\mathrm{m},0}$ also affect the expansion history, and thus the time-redshift relation. Increasing the normalization of the power spectrum, σ_8, boosts the amplitudes of the density perturbations, causing structure to grow earlier. And finally, increasing the spectral index, n_s, boosts the power on small scales relative to large scales, causing haloes to assemble earlier. Without showing the results, we emphasize that the magnitude of this n_s-dependency depends quite strongly on halo mass; it is significantly stronger for low mass haloes with $M_0 = 10^{11}\ h^{-1}\mathrm{M}_\odot$ and becomes negligible for massive clusters with $M_0 = 10^{15}\ h^{-1}\mathrm{M}_\odot$.

All in all, it is clear from Fig. B1 that changes in the cosmological parameters of order 10 percent have a non-neglible impact on the MAHs of dark matter haloes. This motivates
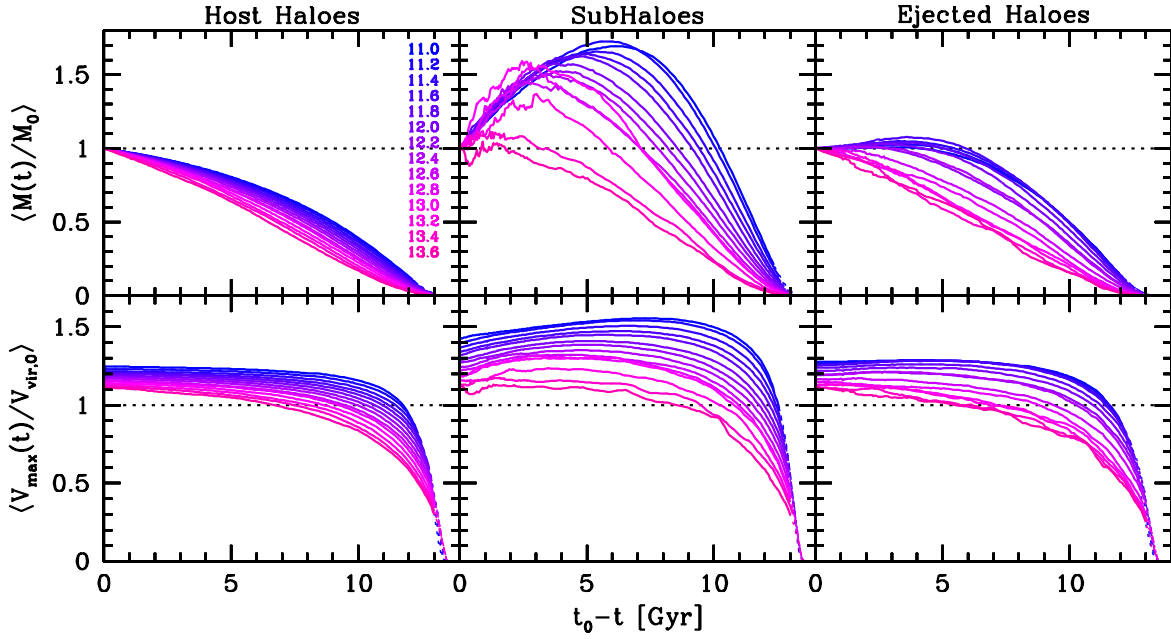
Figure A1. Average MAHs (upper panels) and PWGHs (lower panels) as function of lookback time for host haloes (left), subhaloes (middle) and ejected host haloes (right). Different colors correspond to different present-day halo mass, as indicated in the upper left-hand panel. Note that these different classes of haloes have clearly distinct MAHs and PWGHs. Hence, when studying the behavior of host haloes in numerical simulations, it is prudent to remove subhaloes and ejected host haloes from the sample.
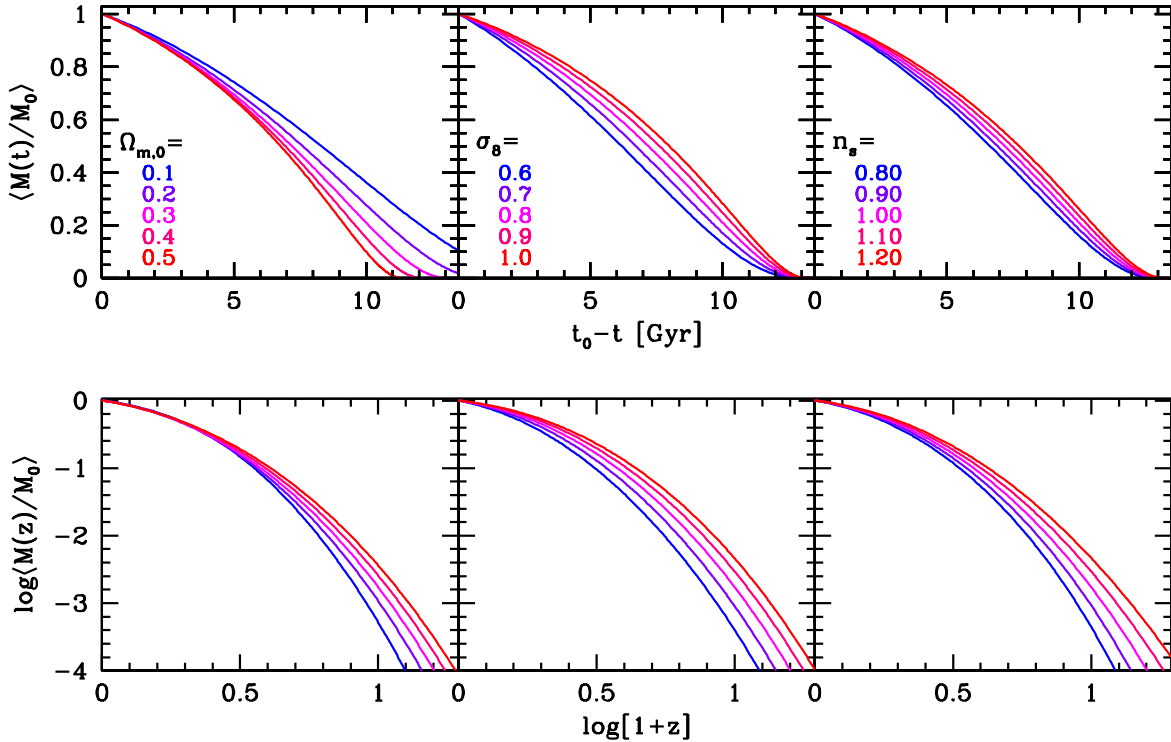

Figure B1. Average MAHs for haloes of mass $M_0 = 10^{13} \, h^{-1} M_\odot$ in different, flat ΛCDM cosmologies. Upper and lower panels plot $\langle M(t)/M_0 \rangle$ as function of lookback time and $\log \langle M(z)/M_0 \rangle$ as function of $\log[1+z]$. Different colors correspond to different cosmologies, where only one cosmological parameter is varied at a time. In the left-hand panel this is $\Omega_{m,0} = 1 - \Omega_{\Lambda,0}$, which is varied from 0.1 to 0.5, in the middle panel σ_8 is varied from 0.6 to 1.0, and in the right-hand panel the spectral index, n_s, is varied from 0.8 to 1.2. See text for a detailed discussion.

the development of universal models, such as that presented in this paper, rather than the use of fitting functions that are only valid for a single cosmology. For the sake of brevity, we do not show how changes in cosmological parameters impact the PWGHs, but this is easily assessed using the Universal model described in §4 and Appendix C.

APPENDIX C: RECIPE FOR COMPUTING MAH AND PWGH

This Appendix details how to compute the average and/or median MAH and PWGH for a host halo of mass M_0 at redshift z_0 in a ΛCDM cosmology.

As described in §4, computing the average or median MAH reduces to numerically solving

$$\mathcal{F}(\psi) = \widetilde{\omega}(\psi, z) \qquad (C1)$$

for ψ at given z, or z at given ψ. Here $\widetilde{\omega}(\psi, z)$ is the universal 'time-coordinate' given by Eq. (19) with $\gamma = 0.4$, and $\mathcal{F}(\psi)$ is a fitting function (Eq. 20) that describes the universal, parametric relation between ψ and $\widetilde{\omega}$. The values for the corresponding parameters are listed in Table 1, and depend on whether ψ represents the average or the median. Note that solving Eq. (C1) for z for a given value of ψ is equivalent to computing the formation redshift z_f for $f = \psi$. Hence, Eq. (C1) can be used to compute the mean or median halo formation redshifts, z_f, for any value of f. This is similar to the model developed by G12, except that our model is valid for main progenitors being defined as the most-massive progenitors, whereas the G12 model corresponds to main progenitors being defined as the most-contributing progenitors (see §2.3).

The following step-by-step procedure outlines how to compute the average (or median) MAH and PWGH:

(i) Define a vector z_i ($i = 1, 2, ..., N$) with the redshifts at which to compute the average or median MAH.
(ii) For each z_i, use a root-finder to solve Eq. (C1) for ψ, and store the resulting values in a vector ψ_i
(iii) For each z_i, use interpolation of ψ_i to find the corresponding $z_{0.04,i}$, defined by $\psi(z_{0.04,i}) = 0.04\,\psi(z_i) = 0.04\psi_i$.
(iv) For each z_i and $z_{0.04,i}$ compute the corresponding proper times, t_i and $t_{0.04,i}$, and use Eq. (14) to compute the halo concentration, c_i, of the main progenitor at z_i.
(v) Use Eqs. (5) and (6) to compute the corresponding PWGH, $V_{\mathrm{max},i}/V_{\mathrm{vir},0}$.

A simple Fortran code that computes the average and median MAHs, PWGHs, mass accretion rates, and main progenitor concentrations as function of redshift is available for download[¶¶]. For a given cosmology, the program takes only a few seconds, on a regular desktop computer, to compute these quantities for tens of halo masses using $N = 400$.

[¶¶] http://http://www.astro.yale.edu/vdbosch/PWGH.html